Md.Mazidul Islam

Wireless sensor based on modulated backscattering principle and LC oscillator

School of Electrical Engineering

Thesis submitted for examination for the degree of Master of Science in Technology.

Espoo, 25.10.2013

Thesis supervisor:

Assistant Professor Ville Viikari

Thesis instructor:

M.Sc. (Tech.) Kimmo Rasilainen

Aalto University
School of Electrical
Engineering

AALTO UNIVERSITY
SCHOOL OF ELECTRICAL ENGINEERING

ABSTRACT OF THE
MASTER'S THESIS

Author: Md.Mazidul Islam

Title: Wireless sensor based on modulated backscattering principle and LC oscillator

Date: 25.10.2013 Language: English Number of pages:11+64

Department of Radio Science and Engineering

Professorship: Radio Engineering Code: S-26

Supervisor: Assistant Professor Ville Viikari

Instructor: M.Sc. (Tech.) Kimmo Rasilainen

This Thesis presents a passive wireless sensor utilizing the modulated backscattering principle. The sensor consists of an antenna, a rectifier, an oscillator, and a modulator. When the sensor is illuminated by a continuous wave (CW), the rectifier generates a DC supply voltage for the oscillator, which drives the modulator. As a consequence, the sensor produces a modulation to the reflected (CW). Sensing can be realized by designing the oscillator such that its frequency depends on the sensed variable.

In this thesis, rectifier, oscillator, and modulator for the transponder are designed and implemented in practice. The operation of each part is analytically predicted using simplified models to anticipate the operation principle of the sensor. Through the analysis, sensor parameters such as rectified DC voltage, oscillator output voltage, power consumption by the oscillator and modulated reflected power of the sensor are predicted. As analytical equations indicate, the modulated reflected power of the sensor can be predicted as a function of input power of the sensor.

It is found out that the rectified DC voltage depends on the diode parameters, input power and load impedance. Oscillator output voltage depends on the rectified DC voltage, oscillator circuit topology, and quality factor and characteristic impedance of the resonator. Moreover, power consumption by an oscillator can be made arbitrarily small by decreasing the capacitive divider ratio. Furthermore, modulated reflected power of the sensor depends on mixer diode parameters, input power of the sensor and output voltage of the oscillator. The operation of all parts are characterized by using simulation and measurement. Simulated and measured results show good agreement, which justifies the accuracy of the results. The developed characteristics are useful for predicting the sensor performance. The results show that the concept is feasible, but further development is needed to obtain a passive sensor with a large read-out distance and smaller power consumption.

Keywords: backscattering, continuous wave (CW), modulator, oscillator, passive sensor, power consumption, read-out distance, rectifier, transponder

Preface

First of all I want to thank the almighty God for strength, guidance and his abundant grace. The work presented in this Master's thesis is based on research carried out in the Wireless Sensors research group of the Department of Radio Science and Engineering (RAD) in Aalto University School of Electrical Engineering between March−September 2013 under the supervision of Assistant Professor Ville Viikari.

My sincere thanks to my supervisor, Professor Ville Viikari for giving me the opportunity to conduct this thesis, and for the advice and support during the work. I would like to thank my instructor M.Sc. (Tech.) Kimmo Rasilainen for his comments regarding my thesis. Also all the other co-workers at the department helped in creating a pleasant working environment. I would like to thank my friends for all the pleasure together.

And last but certainly not least, I would like to express my deepest love and gratitude to my family, especially to my parents. Thank you for all your love, support and encouragement.

Espoo, October 20, 2013,

Md.Mazidul Islam

Contents

Abstract **ii**

Preface **iii**

Contents **iv**

Symbols and abbreviations **vi**

List of Figures **ix**

List of Tables **xi**

1 Introduction **1**

2 Wireless sensors **7**

2.1 Active and semi-passive wireless sensors 7

2.2 Passive wireless sensors 8

2.2.1 RFID 8

2.2.2 Resonance sensors 10

2.2.3 SAW sensors 11

2.2.4 Harmonic sensors 12

3 Oscillator **15**

3.1 Resonator 16

3.1.1 Parallel RLC resonator 16

3.1.2 Series RLC resonator 18

3.1.3 Crystal resonator 19

3.2 Van der Pol oscillator 20

3.3 General analysis 21

3.3.1 Initial condition for oscillation 22

3.4 Frequency stability of an oscillator 25

4 Simplified analytical model for the sensor **27**

4.1 Rectifier 28

4.2 Oscillator 31

4.2.1 Power consumption of an oscillator 31

4.2.2 Output voltage of an oscillator 34

4.3 Modulated power reflected by the sensor 40

5 Experiments **42**
5.1 Rectifier . . . 42
5.1.1 Rectifier prototype . . . 42
5.1.2 Measurement setup . . . 45
5.1.3 Measured and simulated results . . . 46
5.2 Oscillator . . . 48
5.2.1 Oscillator prototype . . . 48
5.2.2 Measurement setup . . . 49
5.2.3 Measured and simulated results . . . 50
5.3 Modulator . . . 52
5.3.1 Modulator Prototype . . . 52
5.3.2 Measurement setup . . . 54
5.3.3 Measured and simulated results . . . 54
5.4 Observation on the experiments . . . 55

6 Conclusion **57**

References **59**

Symbols and abbreviations

Symbols

A	Amplifier gain [dB]
C_{eq}	Equivalent capacitance [F]
$C_j(V_j)$	Junction capacitance at V_j [F]
C_{ox}	Capacitance per unit gate area [F/m^2]
C_p	Parallel RLC resonator capacitance [F]
C_s	Series RLC resonator capacitance [F]
G_L	Conductance of load [S]
g_m	Transconductance [S]
G_m	Large-signal transconductance [S]
$H(\omega)$	Transfer function
I_{bias}	Biased current [A]
i_d	Drain current [A]
$\jmath$	Imaginary unit
I_d	Current waveform [A]
I_s	Saturation current [A]
I_{DC}	Produce diode current [A]
I_{eff}	Effective rms current
K	Boltzmann's constant [J/K]
K_c	Inductive coupling element
K'_n	MOSFET process transconductance parameter
L_p	Parallel RLC resonator Inductance [H]
L_s	Series RLC resonator Inductance [H]
M_{CT}	Circuit structure related parameters
M_I	Mutual inductance
n	Ideality factor
n_c	Capacitive division ratio
P_A	Reflected power by the sensor antenna [W]
P_{in}	Input power of the sensor [W]
P_{Total}	Total power consumption of an oscillator [W]
Q	Quality factor
q	Elementary charge [C]
Q_{reso}	Resonator quality factor

R_a	Antenna resistance [Ω]
R_{bias}	Oscillator bias resistance [Ω]
R_j	Non-linear junction resistance [Ω]
R_p	Parallel RLC resonator resistance [Ω]
R_s	Series RLC resonator resistance [Ω]
S_F	Frequency stability factor
V_a	Voltage across the antenna [V]
V_A	Reflected voltage by the sensor antenna [V]
V_{DC}	Produced diode voltage [V]
V_D	Drain voltage [V]
V_{GS}	Gate-source voltage [V]
V_{osc}	Oscillator output voltage [V]
V_t	Threshold voltage [V]
W_e	Electric field [V/m]
W_m	Magnetic field [A/m]
X	Reactance [Ω]
Z_0	Characteristic impedance of the resonator [Ω]
$Z_{crystal}$	Crystal impedance [Ω]
Z_D	Diode impedance [Ω]
Z_R	Parallel RLC resonator impedance [Ω]
$Z_{resonator}$	Resonator impedance [Ω]
Z_s	Series RLC resonator impedance [Ω]

γ	Profile parameters for depletion capacitance
λ	Wavelength [m]
Φ	Built-in potential for diodes [V]
ω_0	Angular frequency [rad/s]
ω_{rs}	Crystal series angular frequency [rad/s]
ω_{rp}	Crystal parallel angular frequency [rad/s]
ω_{osc}	Oscillator frequency [rad/s]

Abbreviations

AC	Alternating current
ADS	Advanced design system
BJT	Bipolar junction transistor
CW	Continuous wave
DC	Direct current
EM	Electromagnetic
FET	Field effect transistor
HBT	Heterojunction bipolar transistor
HF	High frequency
IC	Integrated circuit
IDT	Interdigital transducer
LF	Low frequency
MEMS	Microelectromechanical systems
MOSFET	Metal-oxide-semiconductor field-effect transistor
PCB	Printed circuit board
RF	Radio frequency
RFID	Radio frequency identification
SAW	Surface acoustic wave
SHF	Super high frequency
UHF	Ultra high frequency
VNA	Vector network analyzer

List of Figures

1.1 The Thing 1
1.2 Existing RFID block diagram and the proposed modification to it. . . 4
2.1 RFID system block diagram. 9
2.2 Backscattering communication principle in an RFID system. 9
2.3 Electrical equivalent circuit for the resonance circuit sensor. 10
2.4 Working principle of the surface acoustic wave (SAW) 12
2.5 Operation principle of harmonic radar and transponder. 13
2.6 Electrical equivalent circuit of the intermodulation sensor device. . . . 14
3.1 General representation of an oscillator circuit. 15
3.2 RLC parallel resonator circuit. 17
3.3 Impedance of a parallel RLC-circuit as a function of frequency relative to resonance frequency for several values of Q. 18
3.4 RLC series resonator circuit. 18
3.5 Simplified electrical equivalent circuit of a crystal resonator. 19
3.6 Van der Pol oscillator. 20
3.7 Four classic oscillator topologies. 22
3.8 Colpitts oscillator. 22
3.9 Small signal electrical equivalent circuit of the Colpitts oscillator. . . 23
3.10 Impedance (Z_R) of parallel resonance circuit. The steepness of the phase slope determines the frequency sensitivity $\frac{\Delta\omega}{\Delta\varphi_0}$ of an oscillator. 26
4.1 Electrical equivalent circuit of the sensor. 27
4.2 Communication principle of the proposed sensor. 28
4.3 The electrical equivalent circuit of an antenna and a rectifier. The antenna is represented as a voltage source. 29
4.4 Colpitts oscillator with bias circuit. 32
4.5 Simplified representation of Colpitts oscillator. 34
4.6 Large signal equivalent circuit of a Colpitts oscillator. 35
4.7 Zeroth order impedance transformation equivalent circuit of the resonator. 35
4.8 Simplified zeroth order impedance transformation equivalent circuit of the Colpitts oscillator. 36
4.9 Simulation model of the oscillator. 38
4.10 Output voltage of the oscillator as a function of input voltage supply predicted by harmonic balance simulation and calculation. 39

4.11 Electrical equivalent model for the reflected and modulated voltage of the sensor. 40
5.1 Schematic circuit of the rectifier simulation model. 44
5.2 Manufactured rectifier prototype. 45
5.3 (a) A schematic layout of the measurement setup for measuring the rectified DC voltage; (b) Measurement setup for characterizing the rectifier. 46
5.4 Measured and simulated reflection coefficient of the rectifier. 46
5.5 Measured DC voltage generated by the rectifier as a function of input frequency. The input power is –10 dBm. 47
5.6 Simulated and measured rectified voltage as a function of the input voltage at 1.085 GHz. 47
5.7 (a) Oscillator simulation model (including losses); (b) Measured Oscillator prototype. 48
5.8 A schematic layout of the measurement setup for measuring the oscillator output. 50
5.9 Comparison between the simulated and measured output voltage of the oscillator as a function of input voltage predicted by harmonic balance simulation. 51
5.10 Measured waveform of the signal when input voltage is 3 V. 51
5.11 Schematic circuit of the modulator simulation model. 53
5.12 Modulator prototype, where the rectifier circuit is also used as a part of the modulator 53
5.13 (a) A schematic layout of the measurement setup for measuring the backscattering response of the sensor; (b) Measurement setup for measuring the backscattering response of the sensor. 54
5.14 Simulated and measured backscattering response of the sensor as a function of output oscillator voltage. The input power is –10 dBm and the oscillation frequency 10 kHz. 55

List of Tables

1.1 The decades of RFID 2
1.2 RFID frequencies and application 3
1.3 Summary of passive wireless sensors 5
4.1 Parameters used in the simulations and calculations 39
5.1 Parameters of the rectifier and modulator circuit used in simulations and measurement 43
5.2 Parameters of the diode (HSMS-2860) 44
5.3 Parameters used in the oscillator simulation and measurement 49

1 Introduction

In recent years, wireless sensors have become an important research area. Possible applications have been identified for example in security, health care, environment monitoring, food safety, robotics and manufacturing industries. Wireless sensors can be divided into battery-powered active devices containing a radio transceiver, semi passive battery-assisted sensors using the modulated backscattering technique for communication, and fully passive sensors [1]. The advantages of passive sensors are that their lifetime or operation conditions are not limited by the power source and that they are inexpensive. Common passive wireless sensors are radio frequency identification (RFID), surface acoustic wave (SAW) RFID, electrical resonance circuit sensors, and harmonic and intermodulation sensors [1]. The Great Seal bug (also known as the "Thing"), an eavesdropping device, is often regarded as the first passive wireless sensor. Fig. 1.1 shows a photograph and a schematical structure of the Great Seal bug.

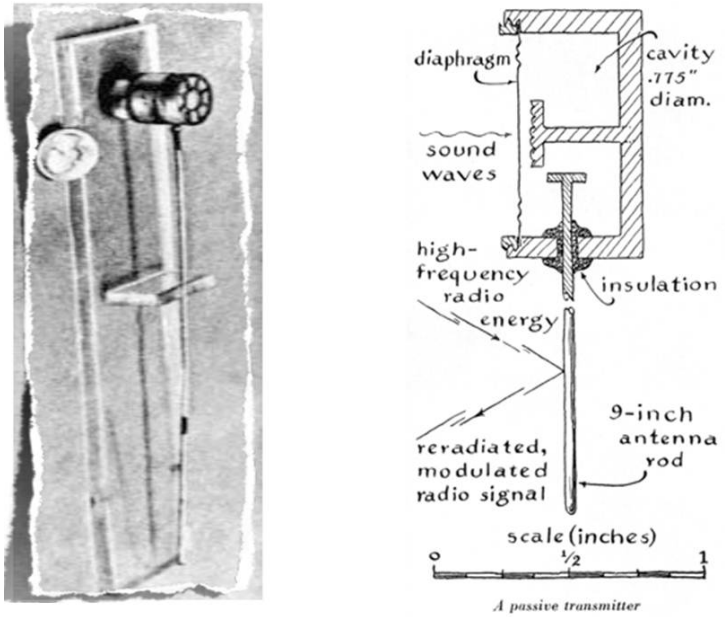

Fig. 1.1: The Thing (from Scientific American,1968).

The device does not have any internal energy source. When it is illuminated with a continuous wave (CW), it reflects a signal modulated with acoustic signal. The device consists of an antenna matched to a capacitive diaphragm microphone. A change in the air pressure due to the sound displaces the diaphragm and alters the capacitance of the microphone. As a consequence, the CW reflects in a different phase from the antenna. The device was designed by Russian inventor Leon Theremin (1896-1993).

Later, the concept of modulated backscattering for communication was proposed by H. Stockman *et al.* in 1948 [2]. Since then, considerable research and development efforts on the topic have led into radio frequency identification (RFID) systems and devices [3]. The development history of RFID is shown in Table 1.1 (reproduced after [4]).

Table 1.1: The decades of RFID [4].

Decades	Event
1940-1950	Radar technology becomes mature due to the research effort made during World War II. Modulated backscattering communication principle is invented in 1948.
1950-1960	Early laboratory experiments of RFID technology.
1960-1970	Some of the landmark inventions and papers are published including "Theory of loaded scatterers" in 1964 [5], "Remotely activated radio frequency power devices," and "Passive data transmission techniques utilizing radar echoes" [6], [7]. The first field trials.
1970-1980	Boom in RFID development. Very early adopters start using RFID.
1980-1990	Commercial RFID applications enter mainstream.
1990-2000	RFID standards emerge. RFID becomes widely deployed.
2000-	RFID has become very important and is ubiquitous in everyday life and in industry. Due to mass production, RFID has become a low-cost technology.

RFID system consist of a reader device and small transponders (or tags) attached to physical objects. Nowadays, RFID is widely used for identification in logistics, smart cards, passports and many other applications. However, RFID could also be used for sensing by adding a sensor element to the tag. Inexpensive and small wireless sensors are needed in places where a wired read-out is difficult due to moving or rotating parts, harsh environment, or due to cost or complexity of cabling. Examples are monitoring of car tire pressure, monitoring of physiological or biological

quantities in animals or humans, and monitoring of moisture in building structures. The main frequency bands allocated for RFID are listed in Table 1.2.

Table 1.2: RFID frequencies and applications [3].

Classification	Frequency Band	Application
LF	120-140 kHz	Access control, Animal ID
HF	13.56 MHz	Access control
UHF	303/433 MHz 866-928 MHz	Transport Transport, Inventory supply chain management
Microwave	2.45 GHz 5.6 GHz	Transport Under development

Low frequency (LF) RFID tags typically operate in the range of 120–140 kHz. Most commonly, LF tags are passively powered through induction. Due to this, they typically have very short read–out ranges of 10–20 centimeters. They can be used in rugged environments and can operate in proximity to metal, liquids, or dirt. This makes them useful for applications like implantable pet identification tags or laundry management tags. LF RFID is quite often used in car immobilization and access control systems. In these systems, a car will only start if a specific LF tag, typically attached to the ignition key, is in proximity to the ignition. This application uses the short read–out distance of LF tags as a security feature.

High frequency (HF) RFID tags operate at a frequency of 13.56 MHz. HF tags are often packaged in a foil inlay or credit card form factor. This makes them useful for building access control, contact-less credit cards, and ID badges. Again, the relatively short read range of HF is an advantage in these applications. HF tags are also used in many asset-tracking applications. Libraries and bookstores often use HF foil inlays to track books. Some airports have started using HF RFID luggage tags for baggage handling application. HF tags offer a higher data rate than LF tags, but do not perform as well as LF tags in proximity to metals or liquids. The HF frequency range lies on a heavily regulated part of the radio spectrum. Signal broadcast by the readers must operate in a narrow frequency band. This presents a problem for environment with sensitive electronics, like medical equipment, that operate on nearby frequencies, making HF tags inappropriate for environments like hospitals.

UHF tags are most commonly used for item tracking and supply-chain management applications. They are largely used because they offer a longer read–out range and are cheaper to manufacture in bulk than LF or HF tags [8]. A major disadvantage of UHF tags is that they experience interference in proximity to liquids or metals. Many applications like animal tracking, metal container tracking, or even many access control systems are infeasible with UHF tags.

Microwave tags operate at either 2.45 or 5.8 GHz. This frequency range is sometimes referred to as super-high frequencies (SHF). Microwave RFID tags are much smaller, more compact and they also offer higher data rate than lower frequency RFID tags. There are several downsides to microwave tags. One is that they consume comparatively more energy than their lower-frequency counterparts. Microwave tags are much more expensive than UHF tags.

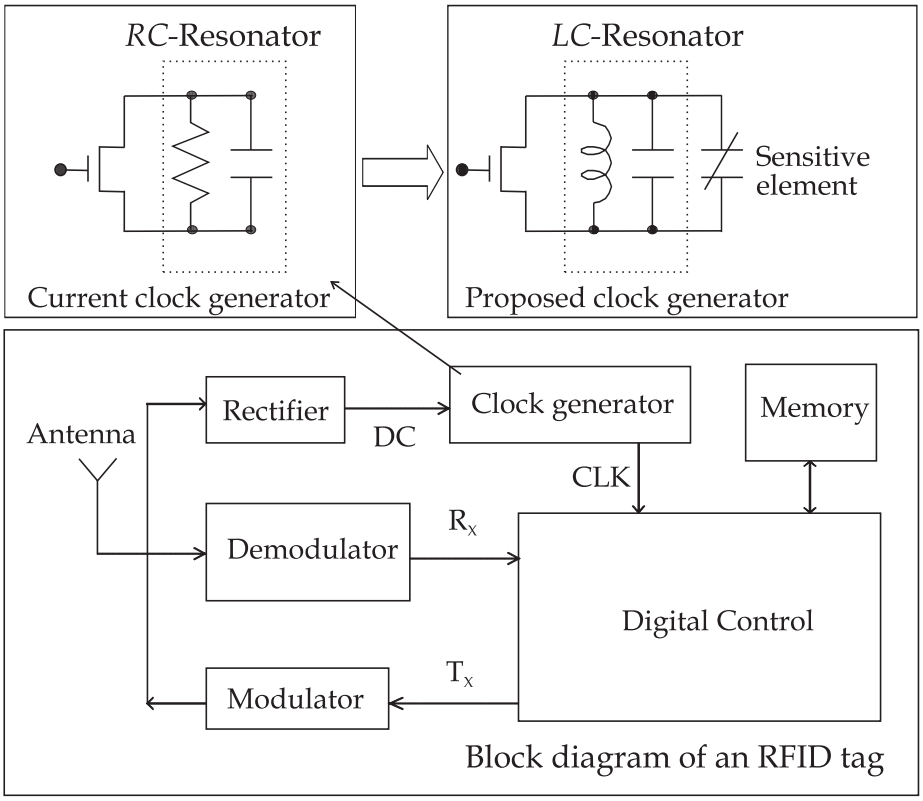

Fig. 1.2: Existing RFID block diagram and the proposed modification to it.

Although the RFID technology is well-established for identification, there are still many competing technologies for sensing purposes. The competing technologies in this field, such as RFID, SAW sensors [9], electrical resonance sensors [10], and harmonic and intermodulation sensors [11], but they all have certain limitations which makes them suitable only for niche applications. No single technology can simultaneously provide sensing, identification, memory, and large read–out distance. For example, when an RFID only sends a number (Tag ID) back to the reader to identify the item, other passive sensors like SAW sensors, electrical resonance sensors, and harmonic and intermodulation sensors are designed to measure physical parameters such as temperature, humidity, pressure and strain.

RFID tags are equipped with a rewritable memory, which enables the reusability features of RFID tags, but they are not useful for measuring external quantities. If an RFID tag is equipped with an external sensor and digital logic to read it, its read-out distance becomes short due to the increased power consumption. On the other hand, SAW sensors, harmonic sensors and intermodulation sensors, can often provide a larger read-out distance but do not provide the sophisticated features of RFID, such as identification and rewritable memory. Table 1.3 summarizes the features related to different passive wireless sensors.

Table 1.3: Summary of passive wireless sensors

sensors features	Resonance sensor	RFID tag	SAW sensor	Harmonic and Intermodulation sensors
ID	No	Yes	Yes	Yes
Rewritable memory	No	Yes	No	No
Sensing	Yes	No	Yes	Yes
Read–out distance	Very small	Large	Very large	Very large

Existing RFID utilizes the inefficient RC-oscillator to realize the clock frequency. The frequency of this oscillator is relatively unstable, its spectral efficiency is poor and it consumes relatively large power. This thesis studies the possibility to equip an RFID tag with an efficient LC-oscillator and an external sensor element. The proposed solution can enable the sophisticated features of RFID with the possibility to measure external quantities without reducing the read-out distance.

The objective of this thesis is to develop a concept for a passive wireless sensor based on modulated backscattering principle and LC oscillator. To describe the operational principle, the sensor is divided in three parts: a) rectifier b) oscillator and c) modulator. The goal is to predict the operation of each part analytically using simplified electrical equivalent models. The analytical equations are verified by simulations and experiments.

This thesis is organized as follows. Chapter 2 presents a general overview on wireless sensors. General theory on oscillators is provided in Chapter 3. In Chapter 4, the operation of the rectifier, oscillator, and modulator are predicted analytically. The experimental results are shown in Chapter 5. Finally, conclusions are given in Chapter 6.

2 Wireless sensors

Sensor is a device that transforms a measured quantity into a readable format, typically into an electrical signal [12]. Nowadays, there are commercially available sensors virtually for any measurement purpose. According to the connectivity, sensors can be divided into wireless and wired sensors. Wired sensors are connected via wiring harnesses or cable assemblies to a reader device. Wireless sensors can be read without a physical connection to the sensor, and are often realized equipping the sensor with a radio transceiver. The transmitted radio signal is interpreted by a receiver which converts the wireless signal into a desired output [13]. Wireless operation can be beneficial in many applications, where wired connection is difficult for example due to harsh operating conditions (like temperature [14] and pressure [15]), rotating parts [16], or cost and complexity of wiring. However, wireless sensors also have some drawbacks such as limited lifetime due to battery, limited read-out distance due to attenuation and interference, security issues because of the uncontrollable propagation of the signal and potentially low speed of communication [17]. Based on the power source and communication principle, wireless sensors can be divided into three categories: active sensors, semi-passive sensors and passive sensors.

2.1 Active and semi-passive wireless sensors

Active wireless sensors usually have both a radio transceiver and an on-board battery that is used to power up the transceiver. Active wireless sensors, having their own power sources, can use powerful transmitters and sensitive receivers. This enables a very long read-out distance [18]. Even a communication range of up to 100 meters can be offered by a low-power transceiver. However, the battery on board limits the life time and also increases the size and weight [19]. Due to more complex circuit, the price of an active sensor can be much higher than that of a passive sensor [20]. Active sensors are widely used in structural health monitoring system for damage detection [21] and they are also applied to monitor active volcanoes (for example Reventador, by Harvard University [22]).

Semi-passive wireless sensors do not contain a radio transceiver, but are equipped with a battery. The battery is used to power up an IC-circuitry and enables the sensors to operate independently of the reader device or to maintain memory in the sensor [3]. Semi-passive battery assisted sensors utilize modulated backscattering technique for communication. This means that semi-passive sensors do not require any power from the on-board battery for transmission, but the sensor simply reflects back some of the power emitted by the reader device [23]. Semi-passive tags are used for monitoring the food chain [24] and environmental variables such as temperature [25].

2.2 Passive wireless sensors

Unlike the active and semi-passive sensors, passive sensors do not require an on-board battery. Therefore they can be less complex, smaller, more inexpensive, and their lifetime is not limited by the power supply. The typical read–out distance of passive wireless sensors is between 10 cm and 3 m [3]. Passive sensor tags are used in medical sector (for example to monitor blood pressure), to monitor moisture in building structures and to monitor temperature in food production [19]. Example of passive wireless sensors are silicon based radio frequency identification (RFID) tags, electrical resonance circuit sensors, surface acoustic wave (SAW) RFID, harmonic sensors and intermodulation sensors [26].

2.2.1 RFID

RFID is an identification technology that uses radio waves to communicate between tags and reader and it is used to identify items. RFID has replaced the barcode technology in many applications. There are a few advantages of RFID over optical barcode identification such as no line-of-sight is required between the reader device and the tag, and the RFID reader can also read hundreds of tags at a time [27]. In [27], it has been forecasted that RFID tags will be widely used for environmental sensing in the near future. Currently, RFID is used in electronic tickets, supply chain monitoring, asset management, and access control [28]. RFID has also been widely used in industrial automation applications because of its big information capacity, high efficiency and security and good reusability [29]. For example, in automobile industry RFID has been used for the body tracking during vehicle production [30].

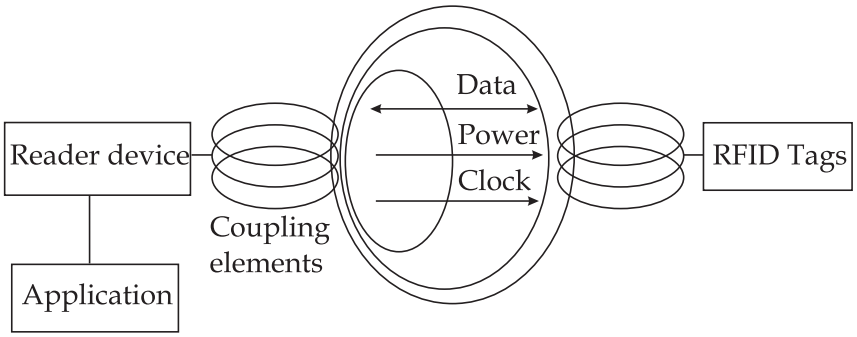

Fig. 2.1: RFID system block diagram.

A typical RFID system is shown in Fig. 2.1, where near-field coupling is used to connect the reader to the tag. When wirelessly interrogated by RFID transceivers, or readers, tags respond with some identifying information. A typical passive tag consists of an antenna connected to an application specific microchip. The tags use the modulated backscattering principle for communication (see Fig. 2.2). In this principle, the RFID tag antenna receives power and RF signals from the RFID reader and sends them to the chip. The chip processes the signals and sends the requested data back to the RFID reader. The backscattered signal is modulated according to the transmitted data. The highest operation frequency and read–out distance of RFID are limited by the rectified power for the integrated circuit (IC) and are a few GHz and 5–10 m, respectively [1]. An additional sensor element further increases power consumption.

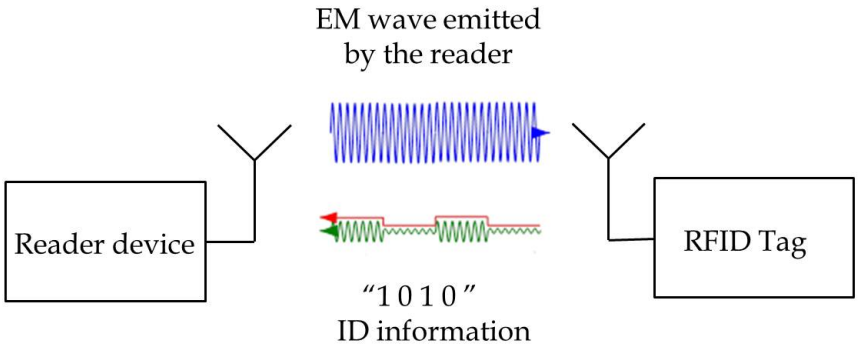

Fig. 2.2: Backscattering communication principle in an RFID system.

2.2.2 Resonance sensors

Resonance sensors consist of a resonator, a reactive coupling element, and a sensor element whose impedance changes according to a measured quantity. An example of an electrical equivalent circuit of a resonance sensor and a reader device coupled to it is shown in Fig. 2.3. The sensor is a series RLC-resonator, whose capacitance is sensitive to the measured quantity. The reader device obtains the state of the sensing element (i.e capacitance) by measuring the impedance of the RLC-resonator. However, the impedance depends on the coupling between the reader and the sensor.

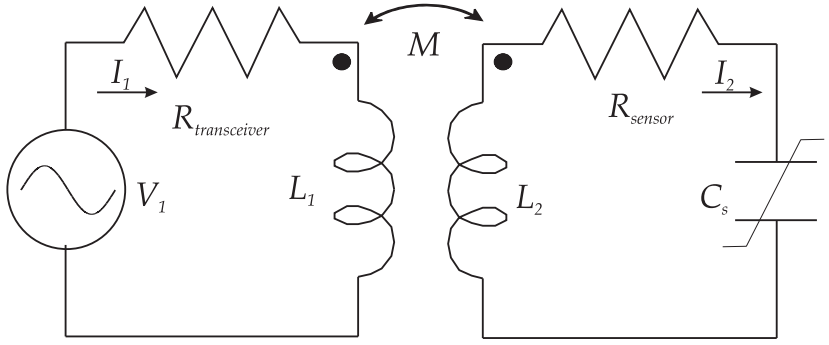

Fig. 2.3: Electrical equivalent circuit for the resonance circuit sensor.

The inductively coupled transceiver and passive sensor can be modeled as the primary and secondary sides of an air-core transformer respectively, with a relatively low inductive coupling coefficient. A mutual inductance relates the two sides so that both sides impose a mutual impedance term on each other. If two air-core inductors are brought near to each other as depicted in Fig.(2.3), the mutual inductance (M_I) between these two inductors is defined as:

$$M_I = K_c\sqrt{L_1 L_2}, \tag{2.1}$$

where K_c is the inductive coupling coefficient. M_I has the unit of inductance and it is the same regardless of which coil is denoted as the primary or the secondary. The voltage (*i.e.* electromotive force) induced by for instance the primary coil on the secondary is then

$$V_{21} = \pm\jmath\omega I_1 M_I, \tag{2.2}$$

where I_1 is the current in L_1. The sign depends on the winding direction of the coils. If an additional impedance Z_2 is connected across the secondary circuit, the

current I_2 becomes:

$$I_2 = \frac{-\jmath\omega I_1 M_I}{Z_2 + \jmath\omega L_2}. \tag{2.3}$$

As a result of mutual inductance, this current in turn induces a voltage on the first coil given by

$$V_{12} = -\frac{I_1 (M_I\omega)^2}{Z_2 + \jmath\omega L_2}. \tag{2.4}$$

The load impedance acting on the primary circuit as a result of the presence of the secondary circuit can be expressed as

$$Z_{12} = \frac{(M_I\omega)^2}{Z_2 + \jmath\omega L_2}. \tag{2.5}$$

The sensor impedance Z_2 in the above equation is the total impedance of the sensor, excluding the inductive reactance of L_2, and including capacitance, resistance and additional parasitic effects. For inductively coupled passive wireless sensors (see Fig 2.3), the capacitance change of the sensor will cause a change in the sensor impedance Z_2. The capacitance change can be obtained wirelessly when the impedance is measured at several frequencies.

A limitation for the resonance sensors is that their read-out distance is only a few centimeters since they require a near field coupling to the reader device [31]. Another limitation of resonance sensors is that their resonance may be affected by proximity to conductive or dielectric objects [32]. Inductively coupled electrical resonance sensors have been used to measure strain [33], moisture [34] and blood pressure [35].

2.2.3 SAW sensors

Surface acoustic wave (SAW) sensors utilize the piezoelectric effect and very low propagation speed of SAW (as compared to that of electromagnetic waves). The operation principle of a surface acoustic wave (SAW) sensor is based on converting an interrogating radio wave from the reader directly into a nano-scale surface acoustic wave on the surface of a piezoelectric substrate. A basic SAW device consist of an interdigital transducer (IDT) with an array of reflectors on a piezoelectric substrate. The IDT consist of a series of interleaved electrodes made of a patterned metal film on a piezoelectric substrate. The operation principle is illustrated in Fig. 2.4. When the antenna of the SAW sensor is interrogated with an RF signal, an electric field is applied to the piezoelectric substrate by the IDT. Then, surface acoustic waves are

generated due to the piezoelectric effect. Next, the waves propagate on the surface of the piezoelectric substrate and partly reflect from the reflective array and travel back to the transducer. Finally, the reflected wave is converted into an electromagnetic wave in the interdigital transducer and is emitted back to the reader by the transponder antenna. The ID is typically coded in the time delays of the different reflections.

Commonly used materials for SAW sensors are quartz (SiO_2), lithium niobate ($LiNbO_3$), and lithium tantalate ($LiTaO_3$) [36]. The SAW propagation properties on piezoelectric substrate depend on the physical quantities like temperature and strain. A change in any of those physical quantities alters the reflected signal. This enables sensing [17]. The advantages of SAW sensors can be high sensitivity and intrinsic reliability. Drawbacks can be relatively large size and short read-out distance due to high acoustic loss [37]. In addition, the need to use piezoelectric material for sensing may limit possible applications. The highest operation frequency is limited by the smallest line of the IDT structure [26], to a few gigahertz.

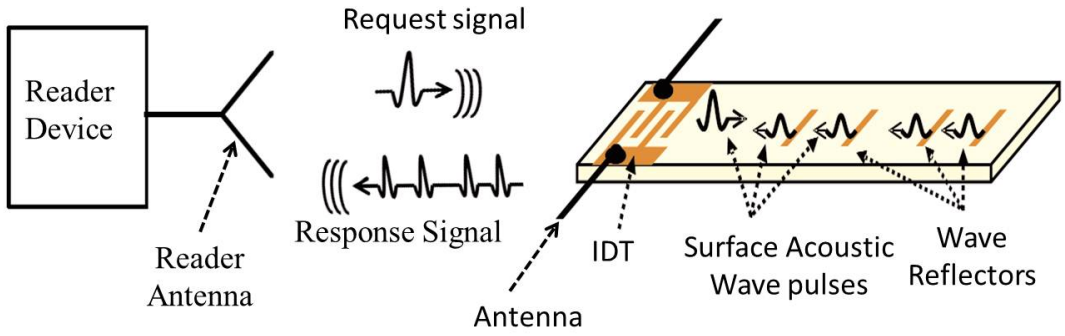

Fig. 2.4: Working principle of the surface acoustic wave (SAW) [38].

2.2.4 Harmonic sensors

Harmonic sensors utilize harmonic frequency conversion for communication. In this principle, the reader actuates the sensor with one or multiple tones. The sensor mixes the tones (nonlinearity is needed in order to set mixing) and reflects a signal containing harmonic products, which are offset from the reader frequencies. The concept is shown in Fig. 2.5. In this example, the harmonic radar transmits a signal that consists of two distinct frequency components (f_1 and f_2). These two frequencies are mixed together in the sensor and a harmonic product is reflected back to

the reader. The harmonic frequencies at $nf_1 \pm mf_2$ are generated in the non-linear element of the sensor. A harmonic reader is a device which illuminates a region of space with RF waves and receives the harmonic of the transmitted frequencies. The received data can then be processed to find the exact location and mobility of the object causing the generation of this harmonic.

Generally, the non-linear element is a diode, a varactor or a MEMS (Microelectromechanical Systems) resonator. The harmonic sensors are typically passive, *i.e.* they only use the energy of the received electromagnetic waves. Although a microwave illumination frequency is mostly used, it has been proposed in [39] that an optical excitation signal can be used for improved spatial localization of the sensor.

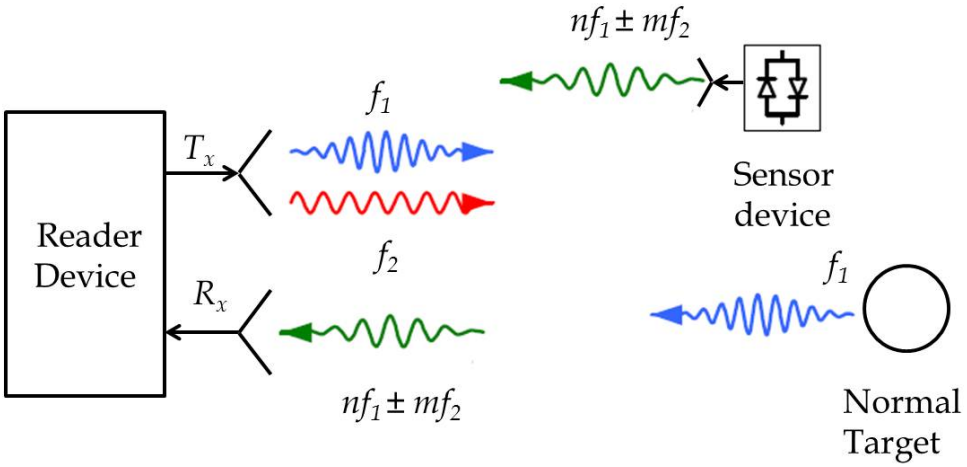

Fig. 2.5: Operation principle of harmonic radar and transponder.

Harmonic radar systems provide an effective modality for tracing insect behavior. They have been used to track insects for 20 years [40]–[46]. This concept was first proposed for a traffic application [47]. Harmonic radars are also used for detecting and identifying vulnerable road users in traffic [48], and for tracking avalanche victims [49].

Intermodulation sensors are one type of harmonic sensors. They utilize an intermodulation frequency for communication. The sensor can be designed so that the intermodulation response is sensitive to a measured quantity. Fig. 2.6 shows an intermodulation sensor, which consists of an antenna matched to a mixing element, and a low frequency resonance circuit. In this principle, the radar transmits a signal containing two frequencies f_1 and f_2 close to each other. The signal received by

the sensor is applied to a mixer which generates current at the difference frequency $f_1 - f_2$. The current at the difference frequency then generates a voltage that depends on the circuit impedance. The voltage at the difference frequency further mixes with the original frequencies, generating an intermodulation signal. The low-frequency resonance circuit contains a sensor element that affects the impedance, and thus the voltage at the different frequency. The sensor data is read out by recording the intermodulation response of the sensor. Intermodulation sensors are presented in [50]–[52]. In general, harmonic and intermodulation sensors can be used at high frequencies and they can provide a large read-out distance [17]. The sensors can also be equipped with an ID. However the concept requires a special reader, and it does not provide memory.

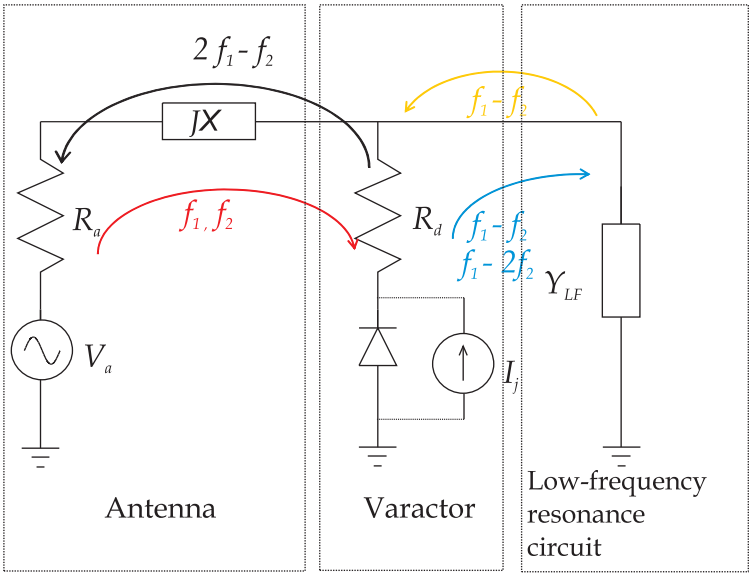

Fig. 2.6: Electrical equivalent circuit of the intermodulation sensor device.

3 Oscillator

In general, an oscillator is a nonlinear circuit that converts DC power to an AC waveform. Fundamentally, an oscillator is an amplifier with a frequency selective positive feedback which has a magnitude greater than one and phase shift equal to a multiple of 2π around the loop [53]. A general representation of an oscillator is shown in Fig. 3.1 where A is the gain of the amplifier and $H(\omega)$ the transfer function of the feedback network.

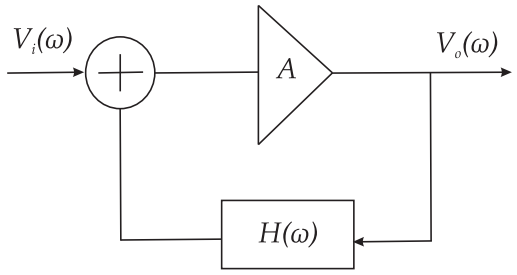

Fig. 3.1: General representation of an oscillator circuit.

The output voltage of the oscillator can be expressed as [54]

$$V_0(\omega) = AV_i(\omega) + AV_0(\omega)H(\omega), \tag{3.1}$$

where V_i is the input voltage. Solving (3.1) for the output voltage gives

$$V_0(\omega) = \frac{A}{1 - AH(\omega)}V_i(\omega). \tag{3.2}$$

According to the Barkhausen criterion, oscillation can be sustained when the loop gain $AH(\omega)$ in steady state equals to unity [53]. The frequency selective feedback of an oscillator is usually realized using a resonator, which can be modeled as a series or parallel RLC circuit. The oscillation frequency may be varied by changing the inductance or capacitance of the resonator.

3.1 Resonator

In a resonance, energy stored in magnetic field (W_m) equals to that stored in electric field (W_e). As a consequence, the impedance of the resonator is real and its absolute value reaches either a local maximum (parallel RLC resonator) or minimum (series RLC resonator) in the resonance. The resonator largely determines the tunability and phase noise properties of an oscillator. The stored energies are also related to the reactance or susceptance. The reactance [55]

$$X = \frac{2\left(W_m - W_e\right)}{|I_{eff}|^2}, \tag{3.3}$$

where I_{eff} is the effective root-mean squared current value. The Q of a circuit can be defined by

$$Q = 2\pi \frac{\text{Energy stored}}{\text{Energy dissipated in one cycle}}. \tag{3.4}$$

Usually, the Q is in interest when there is a resonance, *i.e* $X = 0$ and $W_m = W_m = W$ (as discussed earlier), so (3.4) can be expressed as

$$Q = \frac{2\omega W}{P}, \tag{3.5}$$

where P is the power and ω is the angular resonance frequency. Generally, any resonator can be modeled as series RLC or parallel RLC circuit near the resonance. Crystal resonators have also been widely used in low-frequency (below tens of mega-hertz) oscillators.

3.1.1 Parallel RLC resonator

Fig. 3.2 shows a parallel RLC resonant circuit. The impedance of the circuit is

$$Z_R = \frac{1}{\frac{1}{\jmath\omega L_p} + \frac{1}{R_p} + \jmath\omega C_p}, \tag{3.6}$$

where angular resonance frequency is $\omega_0 = \frac{1}{\sqrt{L_p C_p}}$.

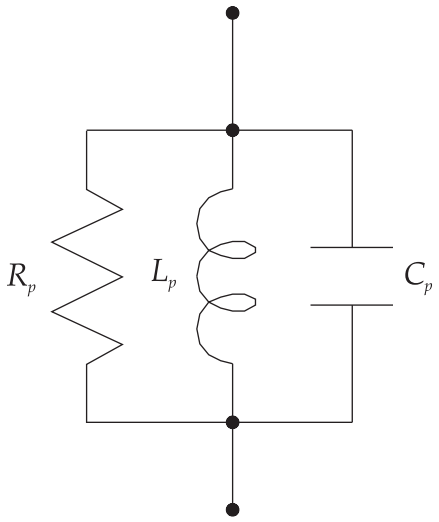

Fig. 3.2: RLC parallel resonator circuit.

Quality factor Q is related to the sharpness of the peak and for parallel RLC resonator, it can be expressed as

$$Q = \frac{R_p}{\omega_0 L_p} = \omega_0 C_p R_p = R_p \sqrt{\frac{C_p}{L_p}}. \tag{3.7}$$

Eq. (3.6) can be expressed in terms of quality factor as

$$Z_R = \frac{R_p}{1 + \jmath \frac{\omega_0}{2Q} \left(\frac{\omega}{\omega_0} - \frac{\omega_0}{\omega} \right)}. \tag{3.8}$$

Fig. 3.3 shows a plot of the magnitude of Z_R as a function of frequency for several values of Q. The plot is normalized to the value of 1 at ω_0 (i.e., $R_p = -13$ dB). The absolute value of the impedance peaks at the resonance. As seen from Fig. 3.3, with the increasing Q of the circuit, the bandwidth becomes smaller and the selectivity of the circuit improves.

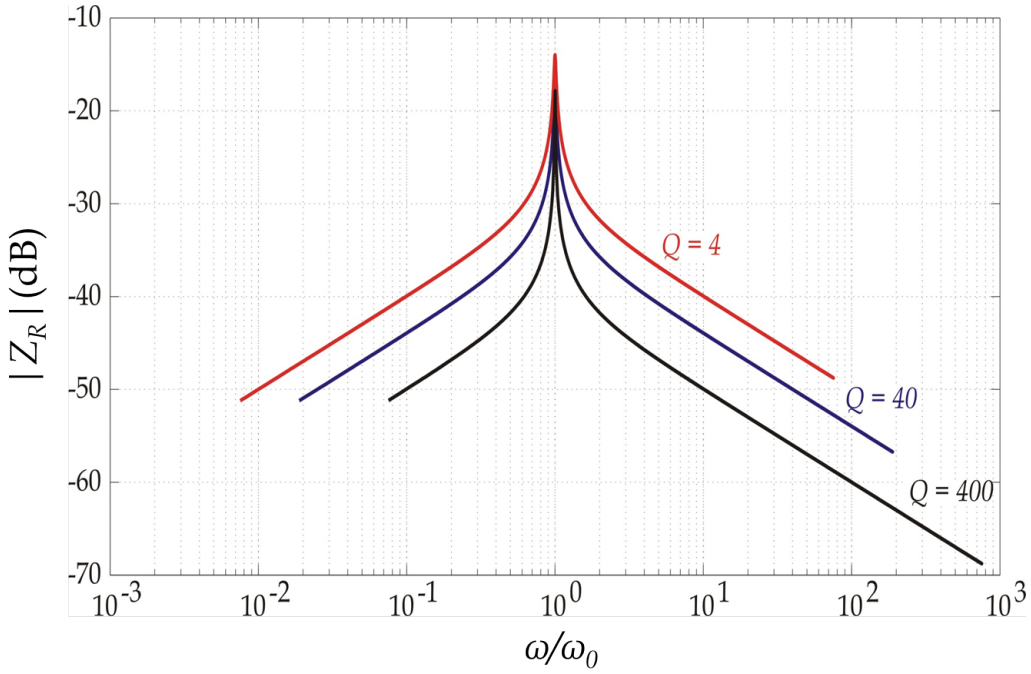

Fig. 3.3: Impedance of a parallel RLC-circuit as a function of frequency relative to resonance frequency for several values of Q.

3.1.2 Series RLC resonator

Fig. 3.4 shows a series RLC resonant circuit. The impedance of the circuit is

$$Z_s = \jmath\omega L_s + R_s + \frac{1}{\jmath\omega C_s} = R_s + \jmath\omega_0 L_s \left(\frac{\omega}{\omega_0} - \frac{\omega_0}{\omega}\right), \tag{3.9}$$

where $\omega_0 = \frac{1}{\sqrt{L_s C_s}}$ is the resonance angular frequency. The bandwidth and selectivity of a series resonator circuit also depend on Q, given for series RLC circuit as

$$Q = \frac{\omega_0 L}{R} = \frac{1}{\omega_0 RC} = \sqrt{\frac{L}{C}}\frac{1}{R}. \tag{3.10}$$

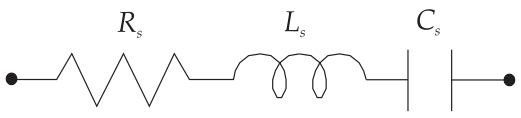

Fig. 3.4: RLC series resonator circuit.

Eq. (3.9) can also be expressed in terms of Q as

$$Z_s = R_s + jQ\left(\frac{\omega}{\omega_0} - \frac{\omega_0}{\omega}\right). \tag{3.11}$$

The absolute value of the impedance is at the minimum in the resonance.

3.1.3 Crystal resonator

Crystal resonators often provide higher Q and thus higher selectivity than electrical resonators. They can also be more stable and less dependent on ambient environment. Crystal resonators utilize a mechanical resonator (*e.g.* quartz crystal), which is coupled to an electrical circuit through a piezoelectric transducer. An electrical equivalent circuit of the crystal resonator is shown in Fig. 3.5, where R_1, L_1 and C_1 represent the motional resistance, inductance and capacitance, respectively, and C_0 represents the parallel capacitance of the crystal.

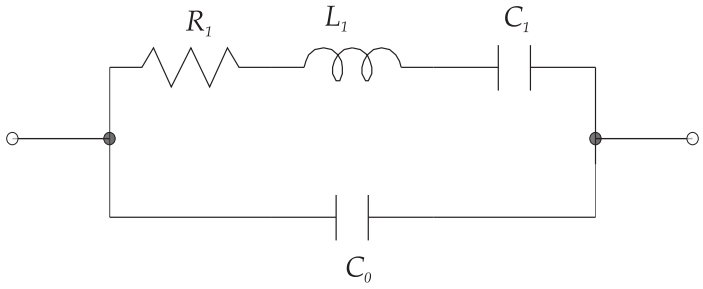

Fig. 3.5: Simplified electrical equivalent circuit of a crystal resonator.

The electrical impedance of a crystal resonator is

$$Z_{crystal} = \frac{\frac{\omega L_1 - \frac{1}{\omega C_1}}{\omega C_0} - \jmath\frac{R_1}{\omega C_0}}{R_1 + \jmath\left(\omega L_1 - \frac{1}{\omega C_1} - \frac{1}{\omega C_0}\right)}. \tag{3.12}$$

When the quality factor is high, the resonance frequency of a crystal resonator is approximately

$$\omega_r \approx \left[\left(\frac{1}{L_1 C_1} + \frac{1}{2L_1 C_0} - \frac{R_1^2}{2L_1^2}\right) \pm \left(\frac{1}{2L_1 C_0} - \frac{R_1^2}{2L_1^2}\right)\right]^{\frac{1}{2}}. \tag{3.13}$$

Eq. (3.13) gives two resonance frequencies; the first, obtained using the minus sign

is the series resonance given as,

$$\omega_{rs} \approx \frac{1}{\sqrt{L_1 C_1}}, \tag{3.14}$$

and the parallel resonance (obtained using the plus sign) is given as

$$\omega_{rp} \approx \sqrt{\frac{1}{L_1 C_1} + \frac{1}{L_1 C_0} - \frac{R_1^2}{L_1^2}}. \tag{3.15}$$

The impedance is inductive between the series and parallel resonance frequencies, and the crystal can be used as an inductor in this frequency range.

3.2 Van der Pol oscillator

Fig. 3.6 shows a simple LC-oscillator first proposed by Balthasar van der Pol in 1920. It consists of an RLC parallel resonator in parallel with an element exhibiting a nonlinear conductance. For simple analysis, assume that the negative conductor follows [56]

$$i = f(v) = -a_1 v + a_3 v^3. \tag{3.16}$$

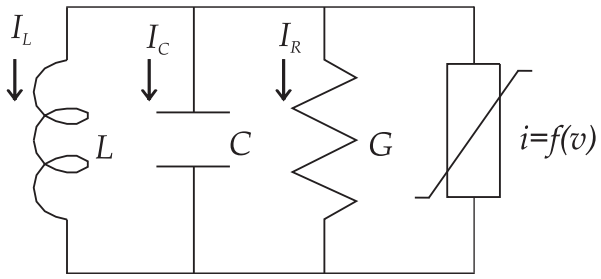

Fig. 3.6: Van der Pol oscillator.

The small signal conductance is $-a_1$, and consequently, the circuit starts to oscillate if $a_1 > G$. According to Kirchhoff's current law, the total current in a parallel circuit must be equal to the sum of the currents in all individual branches, $I_L + I_C + I_R + i = 0$. Taking a derivative with respect to time we get

$$\frac{\mathrm{d}I_L}{\mathrm{d}t} + \frac{\mathrm{d}I_c}{\mathrm{d}t} + \frac{\mathrm{d}I_R}{\mathrm{d}t} + \frac{\mathrm{d}i}{\mathrm{d}t} = 0. \tag{3.17}$$

By substituting the value of $\frac{\mathrm{d}I_L}{\mathrm{d}t} = \frac{v_L}{L}$, $\frac{\mathrm{d}I_c}{\mathrm{d}t} = C\frac{\mathrm{d}^2v}{\mathrm{d}t}$, $\frac{\mathrm{d}I_R}{\mathrm{d}t} = \frac{1}{R}\frac{\mathrm{d}v}{\mathrm{d}t}$ and $\frac{\mathrm{d}i}{\mathrm{d}t} = -a_1\frac{\mathrm{d}v}{\mathrm{d}t} + 3a_3v^2\frac{\mathrm{d}v}{\mathrm{d}t}$ in (3.17) we get

$$\frac{\mathrm{d}^2v}{\mathrm{d}t} + \left[\frac{1}{CR} - \frac{a_1}{C} + \frac{3a_3v^2}{C}\right]\frac{\mathrm{d}v}{\mathrm{d}t} + \frac{v}{LC} = 0. \tag{3.18}$$

Initially, v is very small, and $\frac{3a_3v^2}{C}$ term can be ignored. Eq. (3.18) can be written as

$$\frac{\mathrm{d}^2v}{\mathrm{d}t} + \left(\frac{G - a_1}{C}\right)\frac{\mathrm{d}v}{\mathrm{d}t} + \frac{v}{LC} = 0.$$

The characteristic roots of the corresponding linearized system can be expressed as

$$s^2 + ms + \frac{1}{LC} = 0, \tag{3.19}$$

where $m = \frac{G-a_1}{C}$. So, the poles are $s = -0.5m \pm 0.5\sqrt{m^2 - \frac{4}{LC}} = -0.5m \pm \jmath 0.5\sqrt{\frac{4}{LC} - m^2}$. For, $j\omega$ axis poles, $m = 0$. In the steady-state, the oscillator must fulfill the relation $m = \frac{1}{CR} - \frac{a_1}{C} + \frac{3a_3v^2}{C} = 0$. Amplitude of the oscillation (oscillation frequency $\omega_{osc} = \frac{1}{\sqrt{LC}}$) can be expressed as

$$v = \sqrt{\frac{a_1 - \frac{1}{R_P}}{3a_3}} = \sqrt{\frac{a_1 - G}{3a_3}}. \tag{3.20}$$

Thus, if the amplitude of the oscillator is less than $\sqrt{\frac{a_1-G}{3a_3}}$, then the LC-resonator absorbs energy, and with larger amplitudes it dissipates energy. The oscillation amplitude will stabilize with the balance of dissipation and absorption [54].

3.3 General analysis

Fig. 3.7 depicts four classic oscillators, all invented during the decades after 1900, and named after their inventors. The Colpitts oscillator is perhaps the most widely used oscillator in the history. A simple Colpitts oscillator topology has been chosen to analyze the initial condition for oscillation and minimum power consumption by the oscillator. Colpitts oscillator topology is chosen because it is widely used in commercial signal generators up to 100 MHz and also because it is easy to implement.

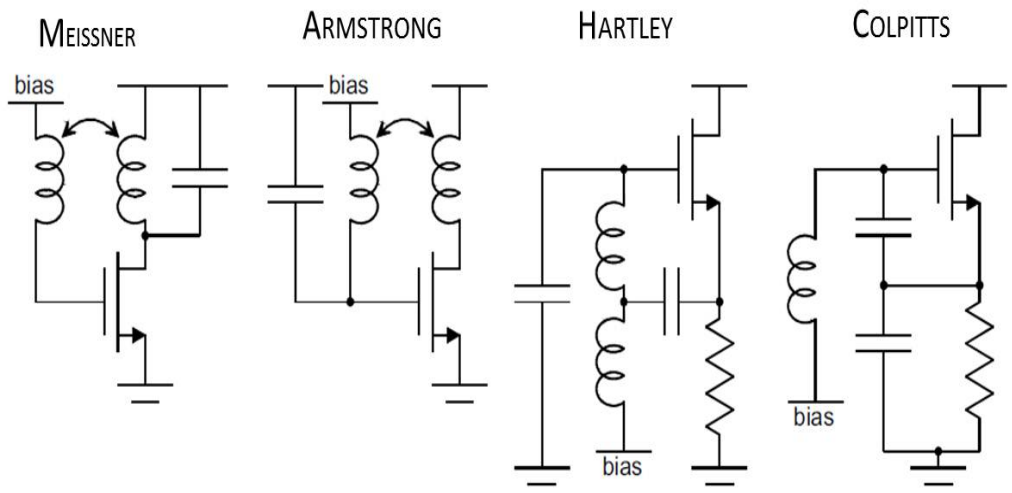

Fig. 3.7: Four classic oscillator topologies [56].

3.3.1 Initial condition for oscillation

Fig. 3.8 shows a Colpitts oscillator without biasing circuits. The required feedback is achieved with a capacitive divider (consisting of C_1 and C_2) in the Colpitts oscillator, and the losses of the inductors, the load resistance, and the output resistance of the transistor are modeled by the resistor R. Assume a low oscillation frequency such that the internal capacitance of the transistor can be neglected. In the following analysis, a BJT transistor is considered.

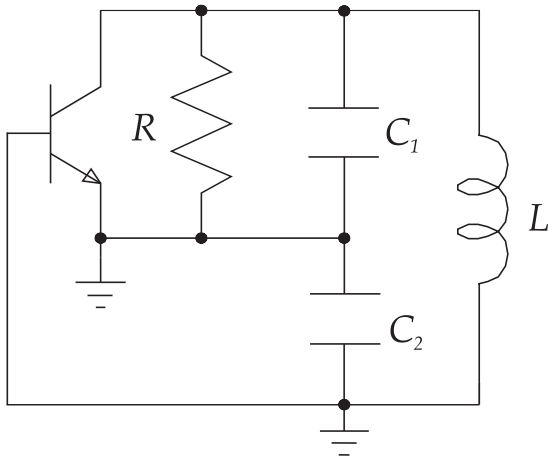

Fig. 3.8: Colpitts oscillator.

The small signal electrical equivalent circuit of the transistor with Colpitts oscillator is depicted in Fig. 3.9.

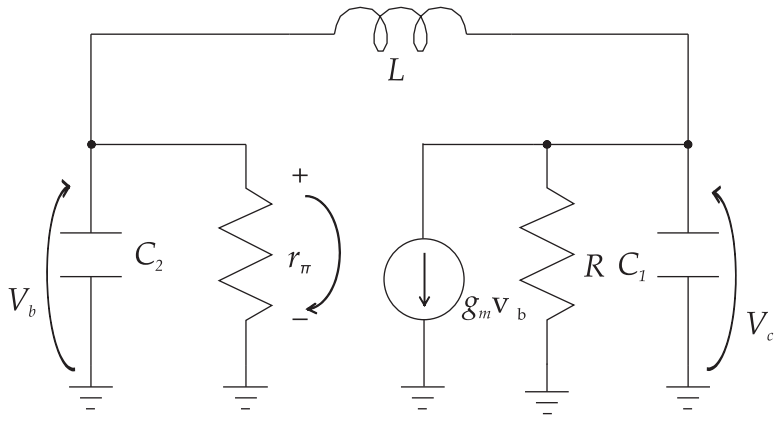

Fig. 3.9: Small signal electrical equivalent circuit of the Colpitts oscillator.

Applying nodal analysis and Kirchhoff's current law at the collector of the transistor gives

$$v_c sC_1 + \frac{v_c}{R} + g_m v_b + \frac{v_c - v_b}{sL} = 0, \tag{3.21}$$

which can be expressed as

$$v_c[s^2 C_1 LR + sL + R] + v_b[sLg_m R - R] = 0, \tag{3.22}$$

and

$$v_b sC_2 + \frac{v_b}{r_\pi} + \frac{v_b - v_c}{sL} = 0, \tag{3.23}$$

from which v_b can be solved to be

$$v_b = \frac{r_\pi}{s^2 C_2 L r_\pi + sL + r_\pi} v_c. \tag{3.24}$$

By substituting the value of v_b into (3.22) we get,

$$s^2 C_1 LR + sL + R + \frac{r_\pi}{S^2 C_2 L r_\pi + sL + r_\pi}[sLg_m R - R] = 0, \tag{3.25}$$

which can be written as

$$[s^2 C_1 LR + sL + R][s^2 C_1 LR + sL + r] + r_\pi[sLg_m R - R] = 0. \tag{3.26}$$

Substituting $s = \jmath\omega_0$ in (3.26) for physical frequency of oscillation and with proper arrangement and separation of the real and imaginary parts, it is possible to obtain

$$\omega_0 = \frac{C_1LR + \frac{L^2}{r_\pi} + C_2LR}{C_1C_2L^2R}, \tag{3.27}$$

and

$$g_mR = \frac{1}{r_\pi}\left(\frac{C_1R}{C_2} + \frac{L}{C_2r_\pi} + \frac{1}{C_1R}\right) + \frac{C_2}{C_1}. \tag{3.28}$$

If MOSFET ($r_\pi = \infty$) is used instead of BJT, then (3.27) and (3.28) can be expressed as

$$\omega_0^2 = \frac{C_1LR + C_2LR}{C_1C_2L^2R} = \frac{C_1 + C_2}{C_1C_2L} = \frac{1}{(C_1||C_2)L}. \tag{3.29}$$

and

$$g_mR = \frac{C_2}{C_1}. \tag{3.30}$$

So, the oscillation frequency and the condition for oscillation can be expressed as

$$f_0 = \frac{1}{2\pi\sqrt{(C_1||C_2)L}}, \tag{3.31}$$

and

$$g_m \geq \frac{C_2}{C_1}G. \tag{3.32}$$

In the above calculation, MOSFET is used instead of BJT because of its simplicity in the analytical solution, and also because its operation requires relatively low power compared with the BJT.

3.4 Frequency stability of an oscillator

Typically a stable oscillation frequency is desired. Frequency stability of an oscillator is analyzed in the following. Using logarithmic differentiation, variations in the tuning capacitance or inductance change the oscillating frequency of the prototype circuit according to [57]

$$\log \omega_0 = -\frac{1}{2}\left[\log C + \log L\right] \Rightarrow \frac{\partial \omega_0}{\omega_0} = -\frac{1}{2}\left[\frac{\delta C}{C} + \frac{\delta L}{L}\right]. \tag{3.33}$$

Typically, variation in ambient temperature affects the stability the most, and therefore one should use components with small thermal coefficient. The frequency stability can be measured in terms of phase variation $\frac{\mathrm{d}\varphi}{\mathrm{d}\omega}$. The frequency stability factor S_F is defined as the ratio between change in phase and relative change in frequency.

$$S_F = \frac{\Delta\varphi}{\left(\frac{\Delta\omega}{\omega_0}\right)} = \omega_0 \frac{d\varphi}{d\omega}|_{\omega=\omega_0}. \tag{3.34}$$

The factor S_F provides a qualitative way for comparing the stability of oscillation. The frequency variation due to a change in the phase is given as

$$\Delta\omega = \omega_0 \frac{\Delta\varphi}{S_F}. \tag{3.35}$$

Fig. 3.10 shows the impedance of a parallel resonance circuit as a function of the frequency. The frequency stability of an oscillator depends on the derivative of phase variation with respect to ω

$$\frac{\mathrm{d}\varphi}{\mathrm{d}\omega} = \frac{\mathrm{d}}{\mathrm{d}\omega}\left(\tan^{-1}\left[Q\left(\frac{\omega}{\omega_0} - \frac{\omega_0}{\omega}\right)\right]\right) = \frac{-\frac{1}{Q}}{\frac{1}{Q^2} + \left[\frac{\omega_0^2 - \omega^2}{\omega_0\omega^2}\right]}\left(\frac{\omega^2 + \omega_0^2}{\omega_0\omega^2}\right). \tag{3.36}$$

In the resonance,

$$\frac{\mathrm{d}\varphi}{\mathrm{d}\omega}|_{\omega=\omega_0} = \frac{-2Q}{\omega_0}. \tag{3.37}$$

The frequency stability factor can be solved by substituting (3.37) into (3.35)

$$S_F = -2Q. \tag{3.38}$$

Eq. (3.38) indicates that the higher is the Q, the smaller is the change in frequency due to a phase change. Consequently, the oscillation frequency will also be more stable.

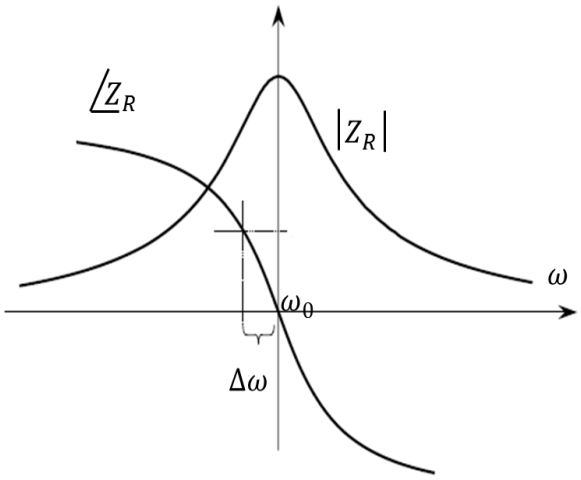

Fig. 3.10: Impedance (Z_R) of parallel resonance circuit. The steepness of the phase slope determines the frequency sensitivity $\frac{\Delta\omega}{\Delta\varphi_0}$ of an oscillator [57].

4 Simplified analytical model for the sensor

The passive RFID tags utilize the modulated backscattering principle for communication. When a tag communicates with a reader, it modulates the received signal and reflects a portion of it back to the reader. The modulation frequency is the same as the clock frequency of the tag. In current RFID systems, the clock is realized with an RC-oscillator whose frequency is relatively unstable. In the following, the feasibility of a passive sensor with an LC-oscillator and sensor element is studied. The oscillation frequency can be made dependent on the sensor element if sensing is required. Therefore, this concept is compatible for existing RFID tags and could enable the possibility to measure external quantities without reducing the read-out distance.

The sensor consists of three main parts: a rectifier, an LC-oscillator, and a modulator. In this chapter, theoretical equations for various properties of the different sensor parts are derived. Fig. 4.1 shows the electrical equivalent circuit of the sensor. The sensor consists of an antenna (represented as a voltage source) matched to a diode, a high pass filter, a low pass filter, a band pass filter and a low frequency oscillator circuit.

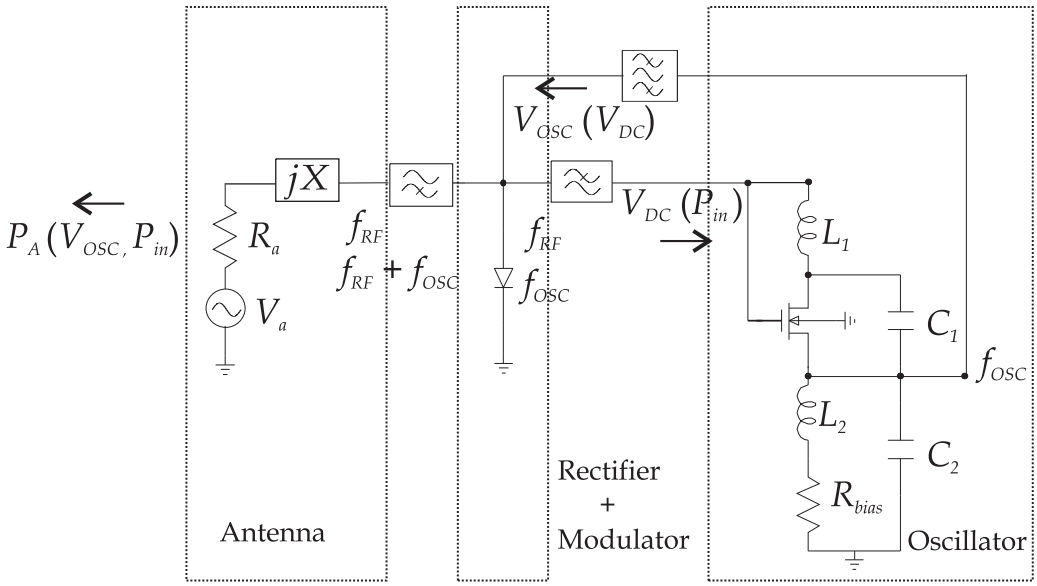

Fig. 4.1: Electrical equivalent circuit of the sensor.

Fig. 4.2 shows the communication principle for the proposed sensor where f_{CW} and f_{OSC} represent the carrier frequency and oscillation frequency, respectively. The sensor is actuated using an RF CW signal. First, the RF signal is converted to DC voltage by a rectifier. The rectified voltage powers up an oscillator, which produces a low frequency sinusoid at its output. Finally, the oscillation signal is fed to the rectifier to realize the backscattering principle. The rectifier modulates the signals, and those going back to the antenna depend on the matching between the antenna and the rectifier. As a consequence, there are sidebands in the signal reflected from the sensor. The sidebands are offset from the carrier by the oscillation frequency. In the following analysis, each part of the sensor will be analyzed separately using simplified models.

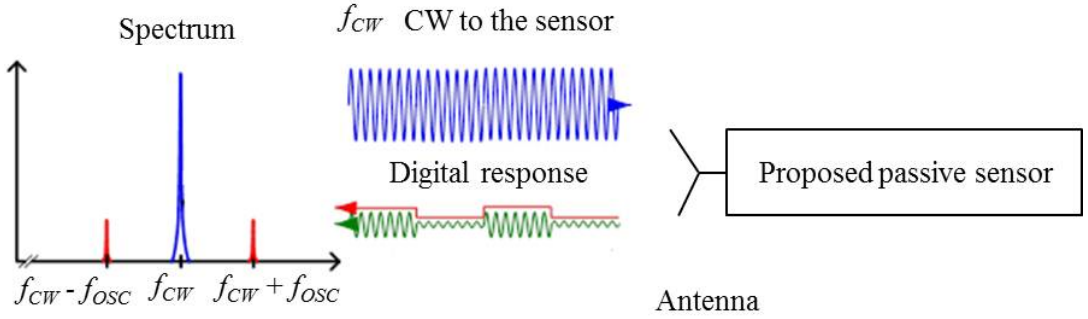

Fig. 4.2: Communication principle of the proposed sensor.

4.1 Rectifier

Rectifiers are based on a non-linear element such as a diode, and they are used to convert AC voltage into DC. The most simple rectifier circuit, which consists of a zero bias Schottky diode, a high-pass filter, a low-pass filter, and a load, is analyzed in this Section. In the rectifier circuit, the oscillator circuit has been considered as the resistive load. Fig. 4.3 shows a rectifier circuit in which an antenna is connected to a diode that is used as the rectifier. The high-pass filter is used as a DC-block, and the low-pass filter is used as an RF choke to prevent RF energy from dissipating in the DC load R_L.

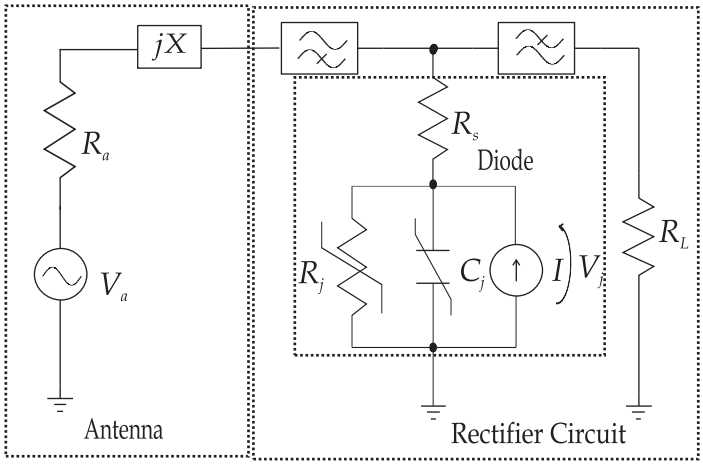

Fig. 4.3: The electrical equivalent circuit of an antenna and a rectifier. The antenna is represented as a voltage source.

The voltage produced by the antenna is given as

$$V_a = 2\sqrt{2P_{in}R_a}\cos\omega_0 t, \tag{4.1}$$

where P_{in} is the power received by the antenna, R_a is the antenna resistance, and ω_0 is the angular frequency of the signal emitted by the reader device. Fig 4.3 shows the electrical equivalent circuit of the diode. I-V curve of the diode is (assuming a Schottky diode)

$$I(V_j) = I_s(e^{j\alpha V_j} - 1), \tag{4.2}$$

where V_j is the voltage across the junction, I_s is the saturation current, $\alpha = \frac{q}{nKT}$ where q is the elementary charge, n is an ideality factor, K is Boltzmann's constant and T is the temperature. Although the series resistance varies slightly with junction voltage, its nonlinearity is usually negligible and it can be treated as a linear element. The voltage-dependent junction capacitance of the varactor is given as

$$C_j(V_j) = \frac{C_{j0}}{(1 - \frac{V_J}{\Phi})^\gamma}, \tag{4.3}$$

where γ is the profile parameter for the depletion capacitance, Φ is the junction potential and C_{j0} is the junction capacitance at zero bias.

At zero bias, the small-signal junction capacitance is

$$C_j \approx \frac{dC_j}{dV_j}|_{V_j=0} = C_{j0}. \tag{4.4}$$

The small-signal junction resistance R_j of the diode is

$$R_j = \frac{1}{\frac{\partial I}{\partial V}}|_{V=0} = \frac{1}{I_s \alpha e^{j\alpha V}} = \frac{1}{I_s \alpha}. \tag{4.5}$$

Assume that the junction resistance dominates the dissipation and that the series resistance can be neglected. Then, voltage across the diode can be written as

$$V_j = \frac{V_a}{R_a + \jmath X + Z_j} Z_D = \frac{V_a}{R_a + \jmath X + R'_j + X'_j} Z_D, \tag{4.6}$$

where Z_D is the diode impedance, R'_j and X'_j are the matching resistance and reactance, respectively. Assuming that the antenna is perfectly matched to the diode ($R_a = \Re\{Z_D\}$ and $X = -\Im\{Z_D\}$), (4.6) can be expressed as

$$V_j = \frac{(1 - \jmath Q)}{2} V_a, \tag{4.7}$$

where Q is the quality factor. Finally, the junction voltage V_j is

$$V_j = \left(\frac{(1 - \jmath Q)}{2} \right) \sqrt{2 P_{in} R_j} \cos \omega_0 t. \tag{4.8}$$

The second-order Taylor's approximation (small-signal approximation) for (4.2) under zero bias is

$$I(V_j) \approx I_s + I_s \alpha V_j + \frac{I_s \alpha^2}{2} V_j^2. \tag{4.9}$$

The linear term of V_j represents the small signal resistance and the square term of V_j contributes to rectification. Let us substitute (4.8) into the last term of (4.9). The current is

$$\begin{aligned} I(V_j) &= \frac{I_s \alpha^2}{2} 2 P_{in} R_j \cos^2 \omega_0 t \left(\frac{(1 - \jmath Q)}{2} \right)^2 \\ &= \frac{I_s \alpha^2}{2} P_{in} R_j \left(\frac{(1 - \jmath Q)}{2} \right)^2 + \frac{I_s \alpha^2}{2} P_{in} R_j \cos 2\omega_0 t \left(\frac{(1 - \jmath Q)}{2} \right)^2. \end{aligned} \tag{4.10}$$

This current can be represented with an equivalent current generator in parallel to the junction. Because of ideal high-pass and low-pass filters, the load impedance to

the generator at DC is $(G_L + R_j^{-1})^{-1}$, and the current is

$$I_{DC} = \frac{I_s \alpha^2}{2} P_{in} R_j \left(\frac{(1 - \jmath Q)}{2} \right)^2 . \tag{4.11}$$

Substituting (4.5) into (4.11) gives the DC current as a function of input power

$$I_{DC} = \frac{1}{2} \alpha P_{in} \left(\frac{(1 - \jmath Q)}{2} \right)^2 . \tag{4.12}$$

The DC voltage produced by the diode can be expressed as

$$V_{DC} = \frac{\alpha P_{in}}{2(\frac{1}{R_j} + G_L)} \left(\frac{(1 - \jmath Q)}{2} \right)^2 , \tag{4.13}$$

where $G_L = R_L^{-1}$, where R_L is the load resistance. The DC voltage produced by the rectifier depends on the diode parameters, input power and the load impedance.

4.2 Oscillator

When used in a passive wireless sensor, an oscillator must produce a large output voltage and its power consumption must be small. The power consumption of a sensor mainly takes place in the oscillator circuit to generate the oscillator output voltage, on which the sensor read-out distance depends. Therefore, power consumption of a sensor can be made arbitrary small by designing an oscillator which can operate with ultra-low supply voltage. Moreover, larger read-out distance of the sensor can be achieved by producing a large oscillator output voltage. In the following, equations for the power consumption and output voltage are derived.

4.2.1 Power consumption of an oscillator

The power consumption of an oscillator depends heavily on the semiconductor fabrication process and transistor technology type. Common processes are silicon (Si), gallium arsenide (GaAs) and silicon germanium (SiGe). Typical technologies used are bipolar junction transistor (BJT), field-effect transistor (FET) and heterojunction bipolar transistor (HBT). The power consumption of an oscillator also depends on the bias circuit and threshold voltage of the transistor. The power consumption

of a simple Colpitts oscillator shown in Fig. 4.4 is calculated.

The metal-oxide-semiconductor field-effect transistor (MOSFET) is a type of field-effect transistor (FET). As compared to BJTs, a MOSFET can be made quite small and its operation requires relatively low power. Therefore, for deriving an analytical equation for the oscillator power consumption MOSFET ($r_\pi = \infty$, see Fig. 3.9) transistor is considered in the following analysis.

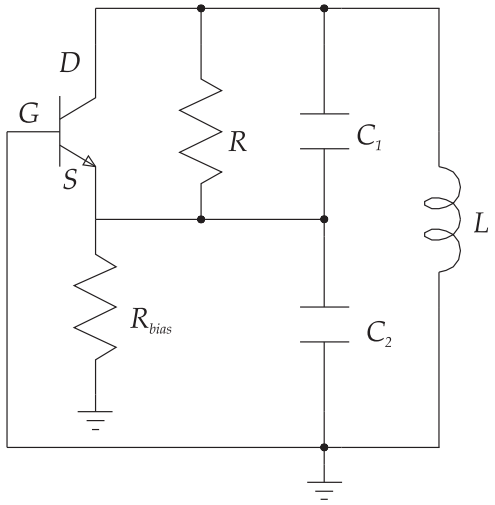

Fig. 4.4: Colpitts oscillator with bias circuit.

Generally, a transistor can operate in three distinct operation regions: the cutoff region, the triode region, and the saturation region. The saturation region is used for amplification purposes. Triode and cutoff regions are utilized in switching [58]. In an oscillator, MOSFET is used as an amplifier and is operated in the saturation region, defined as

$$V_D > V_{GS} - V_t, \tag{4.14}$$

where V_D, V_{GS} and V_t represent the drain voltage, the gate-source voltage and the threshold voltage of a transistor, respectively. Drain current i_d and transconductance g_m of a MOSFET can be calculated from the following equations [58]

$$i_d = \frac{1}{2} K_n{}' \frac{W}{L} \left(V_{GS} - V_t\right)^2, \tag{4.15}$$

$$g_m = K_n{}' \frac{W}{L} \left(V_{GS} - V_t\right), \tag{4.16}$$

where $K_n{}' = \mu_n C_{ox}$ denotes as a MOSFET process transconductance parameter. C_{ox} is known as capacitance per unit gate area and $\frac{W}{L}$ is known as aspect ratio of MOSFET. Eq. (4.17) can be expressed in terms of transconductance g_m as

$$i_d = \frac{1}{2} g_m \left(V_{GS} - V_t\right). \tag{4.17}$$

Consumed power in gate-source(GS) and drain-source(DS) paths are

$$P_{GS} = V_{GS}^2 G_{bias} \tag{4.18}$$

$$P_{DS} = \left(V_D - R_{bias} i_d\right) i_d, \tag{4.19}$$

respectively, the total power consumed by the oscillator is

$$\begin{aligned} P_{Total} &= P_{GS} + P_{DS} \\ &= V_{GS}^2 G_{bias} + \left(V_D - R_{bias} i_d\right) i_d. \end{aligned} \tag{4.20}$$

Requiring operation in the saturation region (4.14) and substituting (4.16) into (4.20), the power can be expressed as

$$P_{Total} = V_{GS}^2 G_{bias} + \frac{K_n' W}{2L} \left(V_{GS} - V_t\right)^3 - \frac{R_{bias} K_n'^2 W^2}{4L^2} \left(V_{GS} - V_t\right)^4. \tag{4.21}$$

Requiring the oscillation condition (4.16), we get

$$V_{GS} \geq \frac{C_2 G L}{C_1 K_n' W} + V_t. \tag{4.22}$$

By substituting (4.22) into (4.21), total power can be expressed as

$$\begin{aligned} P_{Total} \geq \left(\frac{C_2 G L}{C_1 K_n' W} + V_t\right)^2 G_{bias} + \frac{K_n' W}{2L} \left(\frac{C_2 G L}{C_1 K_n' W}\right)^3 \\ - \frac{R_{bias} K_n'^2 W^2}{4L^2} \left(\frac{C_2 G L}{C_1 K_n' W}\right)^4. \end{aligned} \tag{4.23}$$

From (4.23), it can be summarized that the power consumption can be made arbitrarily small by decreasing the ratio $\frac{C_2}{C_1}$ and the bias conductance G_{bias}. As a consequence, however, the output voltage of the oscillator decreases. The output voltage of an oscillator is studied in the following subsection.

4.2.2 Output voltage of an oscillator

A simplified conceptual layout of a Colpitts oscillator without bias circuit is depicted in Fig. 4.5. The two capacitors C_1 and C_2 form a capacitive divider which determines the ratio between the oscillator voltages V_{out} and V_{in}.

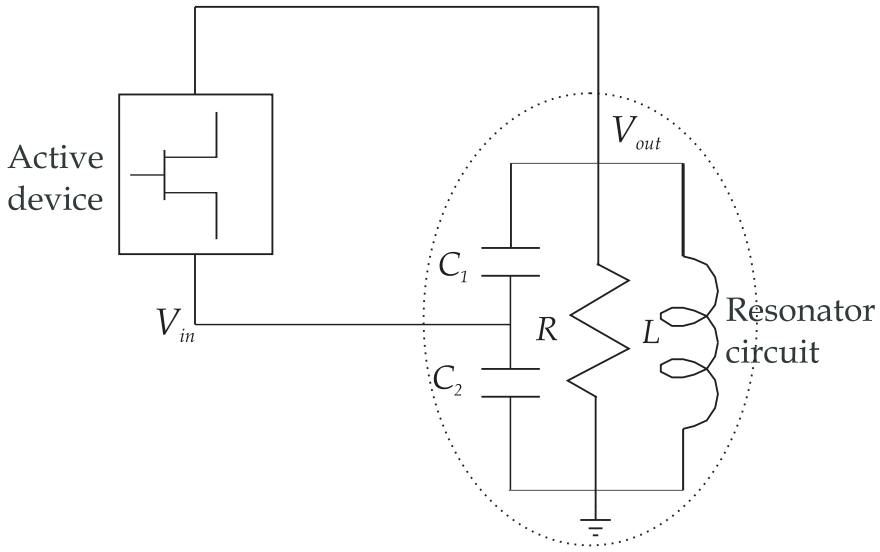

Fig. 4.5: Simplified representation of Colpitts oscillator.

The equivalent capacitance C_{eq} and capacitive division ratio n_c can written as [59]

$$C_{eq} = \frac{C_1 C_2}{C_1 + C_2}.$$
$$n_c = \frac{V_{out}}{V_{in}} = 1 + \frac{C_1}{C_2}.$$

For calculating the output voltage of the oscillator, it is necessary to use a large-signal equivalent transconductance G_m [60]. Let us represent the transistor oscillator with a large-signal equivalent circuit shown in Fig. 4.6.

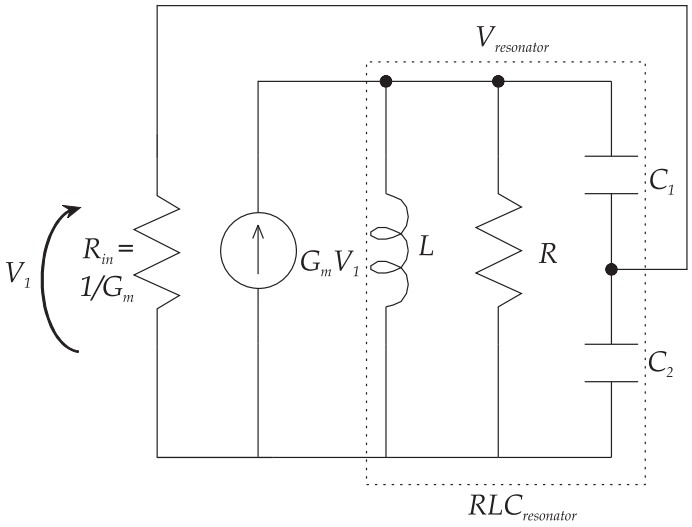

Fig. 4.6: Large signal equivalent circuit of a Colpitts oscillator.

The current that drives the load is $G_m V_1$, and the voltage can be represented as

$$V_{resonator} = G_m V_1 Z_{resonator}, \tag{4.24}$$

where $Z_{resonator}$ is the impedance of the resonator. There are useful transformations that allow us to move between parallel and series combination of RC and LC, which are known as zeroth order impedance transformations [60]. Let us consider zeroth order impedance transformation to find out the impedance of the resonator ($Z_{resonator}$).

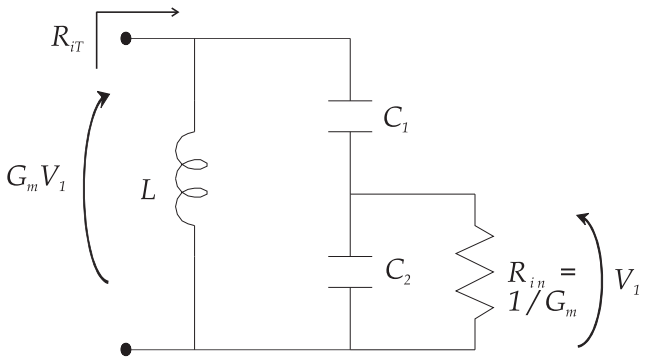

Fig. 4.7: Zeroth order impedance transformation equivalent circuit of the resonator.

A Zeroth order impedance transformation equivalent circuit is shown in Fig. 4.8, where R_{iT} derives from the impedance transformation and R_{in} depends on the ca-

pacitance divider. Two capacitors (or inductors) in series act like a "transformer" for impedances which can be represented as,

$$\left(\frac{R_{iT}}{R_{in}}\right)^{\frac{1}{2}} = \frac{1}{n_c}$$
$$\Rightarrow R_{iT} = \frac{1}{n_c^2 G_m}. \tag{4.25}$$

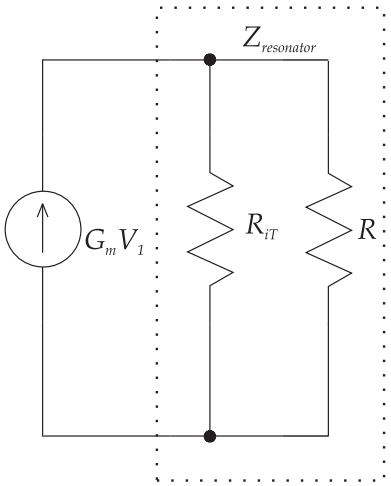

Fig. 4.8: Simplified zeroth order impedance transformation equivalent circuit of the Colpitts oscillator.

Therefore the impedance $Z_{resonator}$ can be written as,

$$Z_{resonator} = R||R_{iT} = R||\frac{1}{n_c^2 G_m} = \frac{R}{1 + n_c^2 G_m}.$$

By substituting the value of $Z_{resonator}$, (4.24) becomes

$$V_{resonator} = \frac{G_m V_1 R}{1 + n_c^2 G_m}. \tag{4.26}$$

Hence, the output voltage of an oscillator is

$$V_{osc} = n_c V_{resonator} = \left(1 + \frac{C_1}{C_2}\right) G_m V_1 \left(\frac{R}{1 + n_c^2 G_m}\right). \tag{4.27}$$

In the simplified case, it is considered that a basic Colpitts oscillator is biased with an ideal current source I_{bias}. The active device has a current waveform $I_d(t)$, and

the amplitude of the fundamental tone can be obtained from the Fourier series representation [61]. The average current must be equal to

$$\langle I_d \rangle = \frac{1}{T}\int_0^T I_d(t)\ \mathrm{d}t = I_{bias}.$$

The fundamental component of drain current is

$$I_1 = \frac{2}{T}\int_0^T I_d(t)\cos\omega_{osc}\ \mathrm{d}t.$$

If $I_d(t)$ is a narrow pulse or actually a chain of pulses, these pulses appears at the maximum point of oscillation, and so we may approximate the cosine term by unity. Furthermore, over the complete oscillation period the overall signal current must be equal to I_{bias}. Therefore

$$I_1 = \frac{2}{T}\int_0^T I_d(t)\cos\omega_{osc}\ \mathrm{d}t \approx \frac{2}{T}\int_0^T I_d(t)\ \mathrm{d}t \approx 2I_{bias}.$$

The large-signal G_m can be calculated from

$$G_m = \frac{I_1}{V_1} = \frac{2I_{bias}}{V_1}. \tag{4.28}$$

The output voltage of the oscillator can be expressed as

$$V_{osc} = \left(1 + \frac{C_1}{C_2}\right) 2I_{bias} \left(\frac{R}{1 + n_c^2 G_m}\right). \tag{4.29}$$

When $1 + n^2 G_m \approx 1$, the oscillation voltage is

$$\begin{aligned} V_{osc} =& \left(1 + \frac{C_1}{C_2}\right) 2I_{bias}R \\ =& 2\left(\frac{1}{1 + \frac{C_2}{C_1}}\right) I_{bias}R\sqrt{\frac{C_1||C_2}{L}}\sqrt{\frac{L}{C_1||C_2}}. \end{aligned} \tag{4.30}$$

This result can be represented as

$$V_{osc} = M_{CT} I_{bias} Q_{resonator} Z_0, \tag{4.31}$$

where $M_{CT} = 2\left(\frac{1}{1+\frac{C_2}{C_1}}\right)$, $Q_{resonator} = R\sqrt{\frac{C_1||C_2}{L}}$ and $Z_0 = \sqrt{\frac{L}{C_1||C_2}}$. This is the generalized oscillator output voltage formula. Here M_{CT} is the factor carrying information on circuit topology, design choices and active device characteristics. $Q_{resonator}$

is the quality factor of the resonator and Z_0 represents the characteristics impedance of the resonator. Eq. (4.31) is verified by simulation, in which a simple Colpitts oscillator is analyzed. A MOSFET with parallel resonator Colpitts oscillator is designed and a low voltage Colpitts oscillator is presented in Fig. 4.9. This oscillator can operate at the supply voltage above 4 mV. For the design of the oscillator, a MOSFET (ALD800) with a very low threshold voltage has been used.

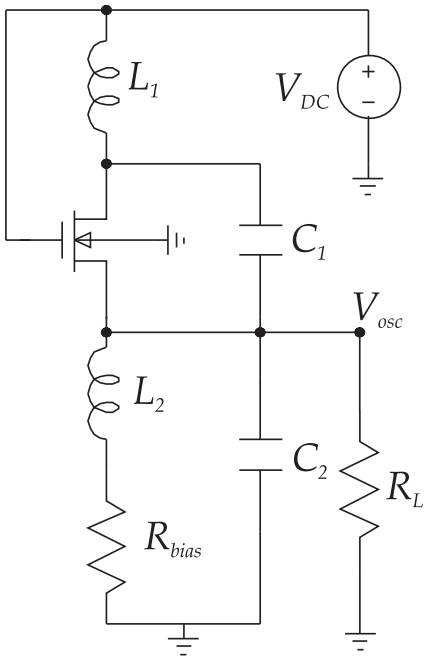

Fig. 4.9: Simulation model of the oscillator.

The circuit contains a common-gate amplifier, including capacitive divider composed of C_1 and C_2, a feedback inductor L_1 and a load resistance R_L. For ultra-low-voltage operation, the transistor terminals are connected to the supply voltage V_{DD} and to the ground via inductors L_1 and L_2 and biasing resistance R_{bias}. The oscillator response is simulated with the ADS simulator (Agilent Technologies, Santa Clara, CA [Online]. Available : http://web.agilent.com/) by harmonic balance simulation, using the transistor SPICE (LEVEL 2) model obtained from the manufacturer (Advanced Linear Devices, INC.). The component values used in the simulation and calculation are listed in Table 4.1.

Table 4.1: Parameters used in the simulations and calculations

Feedback inductor	$L_1 = 1$ mH
Bias inductor	$L_2 = 10$ mH
Capacitor	$C_1 = 3.3$ nF
Capacitor	$C_2 = 16$ nF
Load resistance	$R_L = 0.5$ MΩ
Feedback resistance	$R_{bias} = 50$ Ω

The analysis of the oscillator assumes that the transistor is operating under the saturation condition and neglects the transistor output conductance [57]. The calculated and simulated output voltage of the oscillator as a function of input voltage is shown in Fig. 4.10. For calculating the oscillation output voltage with (4.31), I_{bias} current is calculated from the simulation as a function of input voltage supply. Fig. 4.10 exhibits a good shape agreement between the simulated and calculated curves, but there is some horizontal offset between the voltages. The oscillator output voltage equation is derived in approximative manner, which might explains the observed horizontal offset between the analytical and simulated curves.

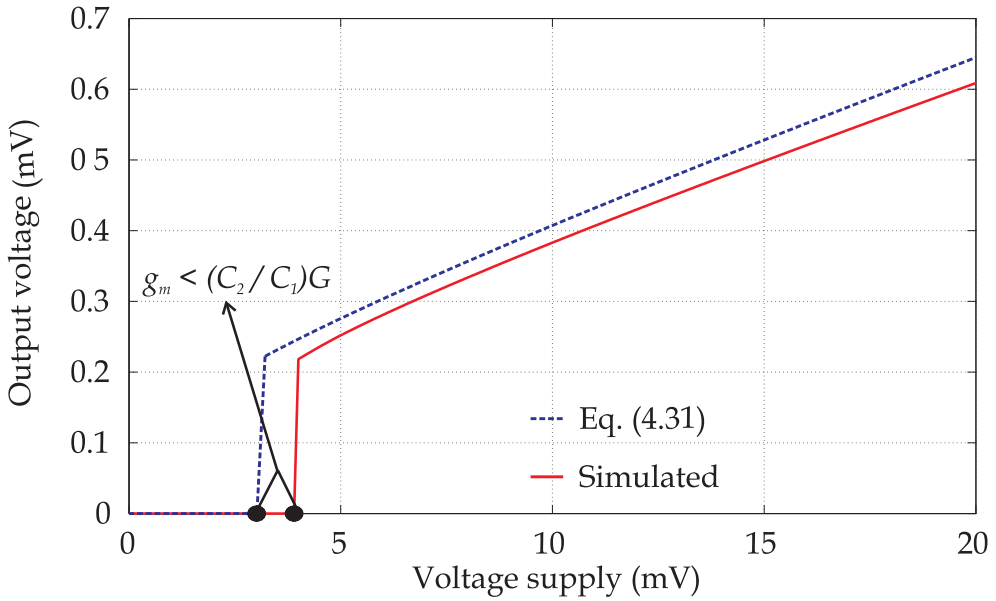

Fig. 4.10: Output voltage of the oscillator as a function of input voltage supply predicted by harmonic balance simulation and calculation.

Calculating the I_{bias} current necessitates that the transconductance is known. In practice, the transconductance in not always provided by the manufacturer and the current consumption must be simulated.

4.3 Modulated power reflected by the sensor

As was discussed earlier, the sensor utilizes the modulated backscattering principle for communication. The modulated backscattering is realized by applying the oscillator output to the rectifier. In the modulator, the rectifier diode is used as a mixer. The oscillation signal modulates the RF impedance of the rectifier. As a consequence, there are sidebands in the signal reflected from the sensor. Fig. 4.11 shows a simplified model that will be used to derive an equation for the reflected signal from the sensor at a sideband. The antenna and the oscillator are represented as voltage sources. The signals from both sources are mixed in the diode, which generates current at the difference frequency.

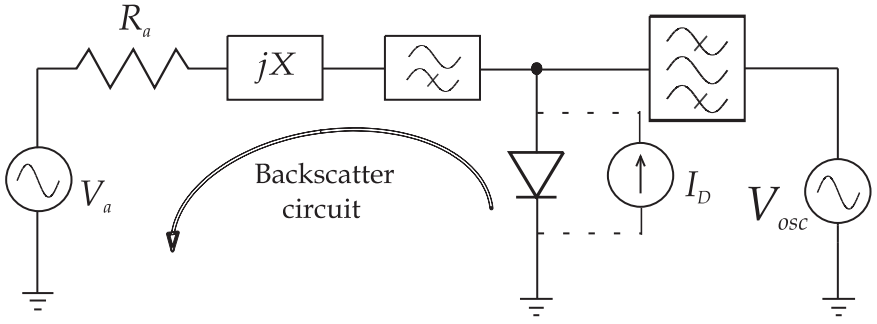

Fig. 4.11: Electrical equivalent model for the reflected and modulated voltage of the sensor.

Following the analysis of Section 4.1, the current generated by the diode can be written as

$$\begin{aligned} I_D &= \frac{\alpha}{2R_j}(V_{osc}\cos\omega_{osc}t + \sqrt{2P_{in}R_j}\cos\omega_0 t)^2 \\ &= \frac{\alpha}{2}V_{osc}^2 P_{in}[\cos(\omega_0 - \omega_{osc}) + \cos(\omega_0 + \omega_{osc})], \end{aligned} \tag{4.32}$$

where V_{osc} is the oscillator output voltage and ω_{osc} is the oscillation frequency. Let us consider only the lower side band in the following. The current at the difference frequency then generates a voltage that depends on the circuit impedance. The

difference frequency is in the pass band of the high-pass filter and in the stop band of the low-pass filter. The voltage at the oscillation frequency mixes with the original input frequency, generating signals at the sum ($\omega_0 + \omega_{osc}$) and difference ($\omega_0 - \omega_{osc}$) frequencies. The reflected voltage by the antenna (considering lower side band) can be expressed as

$$V_A = \frac{\alpha R_j V_{osc}^2 P_{in}}{4} \cos\left[(\omega_0 - \omega_{osc})t\right]. \tag{4.33}$$

The reflected power by the antenna can be represented as

$$P_A = \frac{\alpha^2 R_j^2 V_{osc}^4 P_{in}^2}{16 R_a}. \tag{4.34}$$

The reflected power by the sensor depends on the diode parameters, sensor input power, oscillator output voltage and the internal resistance of the antenna.

5 Experiments

In this chapter, the three parts of the prototype sensor are implemented and tested separately. The parts are the rectifier, the oscillator and the modulator. The simulated and measured results are also compared for each individual part to ensure that the analytical and simulation models are relevant. Each part of the sensor performance is characterized to predict the overall sensor performance.

5.1 Rectifier

When the sensor is illuminated with a continuous wave (CW), the rectifier circuit produces the DC voltage for the oscillator operation. A simple rectifier consisting of an antenna matching circuit, a diode and a load is implemented. The antenna is isolated from the rectifier diode with the DC block capacitance, and the load is isolated from the antenna at RF with an RF choke. The rectifier is realized using surface mounted components separated with microstrip line sections to facilitate soldering of the components.

5.1.1 Rectifier prototype

The rectifier was simulated with the ADS software using the harmonic balance simulation. Harmonic balance is typically used to simulate circuits with non-linear elements under harmonic steady-state excitation. Fig. 5.1 shows the circuit schematic of the rectifier simulation model. In simulation, real component models by Murata are used to predict the rectifier response. When the simulation has been carried out, the OSC port is kept open and the DC port is connected with a load. The component values used in the simulation and measurement are listed in Table 5.1.

Table 5.1: Parameters of the rectifier and modulator circuit used in simulations and measurement

Antenna resistance	$R_a = 50\ \Omega$
Matching inductor (LQW18AN11NG00)	$L_m = 11$ nH
Matching capacitor (GQM1875C2E120JB12)	$C_m = 12$ pF
Low-frequency block capacitor (GQM1885C2A2R0BB01))	$C_H = 2$ pF
RF block inductor (LQW18AN43NG00)	$L_{low} = 43$ nH
Band-pass filter inductor (LQW18AN43NG00)	$L_{mlow} = 43$ nH
Load resistance	$R_L = 0.5\ \text{M}\Omega$
Transmission line (TL_1)	$l = 30$ mm $w = 2.3$ mm.
Transmission line (TL_2)	$l = 9.8$ mm $w = 2.3$ mm.
Transmission line (TL_3)	$l = 14.3$ mm $w = 10$ mm.
Transmission line (TL_4)	$l = 4.68$ mm $w = 2.3$ mm.
Transmission line (TL_5)	$l = 4.675$ mm $w = 2.3$ mm.
Transmission line (TL_6)	$l = 5$ mm $w = 2.3$ mm.
Transmission line (TL_7)	$l = 5$ mm $w = 2.3$ mm.
Transmission line (TL_8)	$l = 10$ mm $w = 10$ mm.
Transmission line (TL_9)	$l = 4.7$ mm $w = 2.3$ mm.
Transmission line (TL_{10})	$l = 20$ mm $w = 10$ mm.
Transmission line (TLM_1)	$l = 7.2$ mm $w = 2.3$ mm.
Transmission line (TLM_2)	$l = 30$ mm $w = 10$ mm.
T-junction transmission line ($TL_1 = TL_2 = TL_3 = w$)	$STL_1(w) = 2.3$ mm
junction transmission line ($TL_6 = TL_7 = TL_9 = TLM_1 = w$)	$STL_2(w) = 2.3$ mm

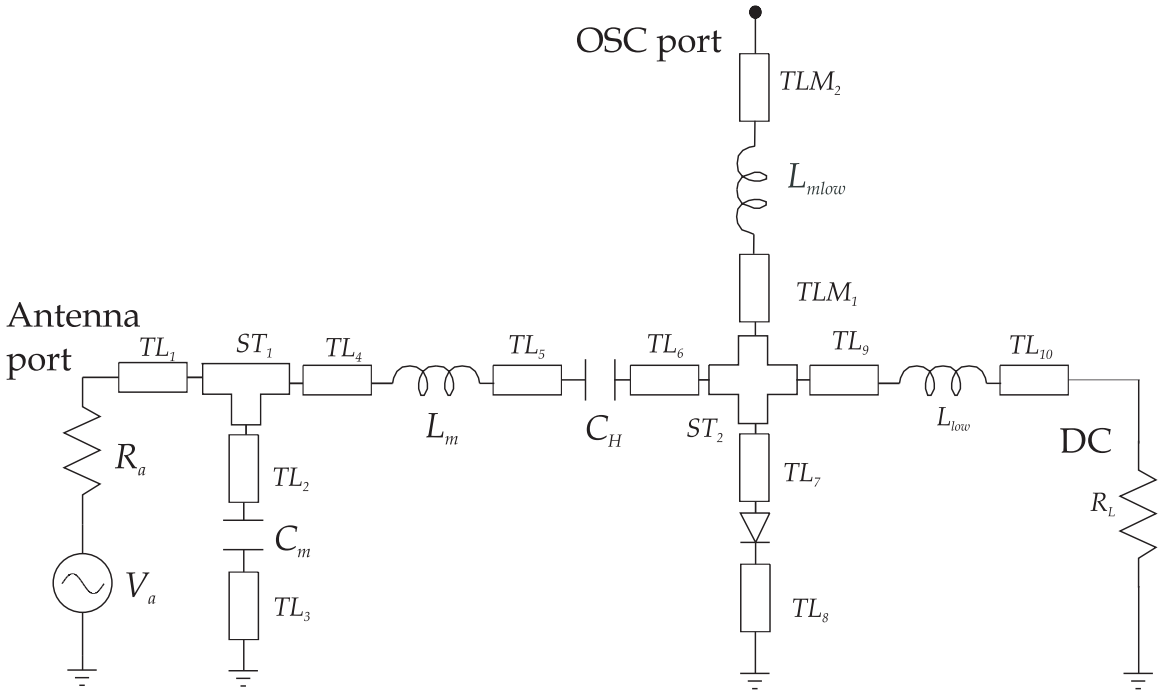

Fig. 5.1: Schematic circuit of the rectifier simulation model.

In the rectifier circuit, lumped capacitor C_m and inductor L_m are used as matching elements and a zero bias Schottky diode as a rectifier. The 2 pF capacitor C_H is used as a high-pass filter which isolated the rectifier circuit from the antenna and the 43 nH inductor L_{low} is used as a low pass filter to prevent RF signal accessing the load. A zero bias Schottky diode HSMS-2860 by Avago Technologies is used for rectification. The diode parameters are shown in Table 5.2.

Table 5.2: Parameters of the diode (HSMS-2860) [62].

Junction capacitance	$C_{j0} = 0.18$ pF
Saturation current	$I_s = 50$ nA
Ideality factor	$n = 1.08$
Series resistor	$R_s = 6\ \Omega$
Junction grading coefficient	$M = 0.5$

The rectifier prototype was manufactured to experimentally verify the simulated model of the rectifier. For that purpose, a circuit layout has been generated with the ADS software and fabricated in the Department of Radio Science and Engineering laboratory. ROGERS RT/duroid 5870 ($\varepsilon_r = 2.33$, $\tan\delta = 0.0012$) is used as the substrate for the rectifier PCB design. The rectifier prototype is implemented with lumped circuit elements soldered on the PCB. To realized the antenna in practice, a 50 Ω SMA connector is soldered in the antenna port. The photograph of the prototype is shown in Fig. 5.2.

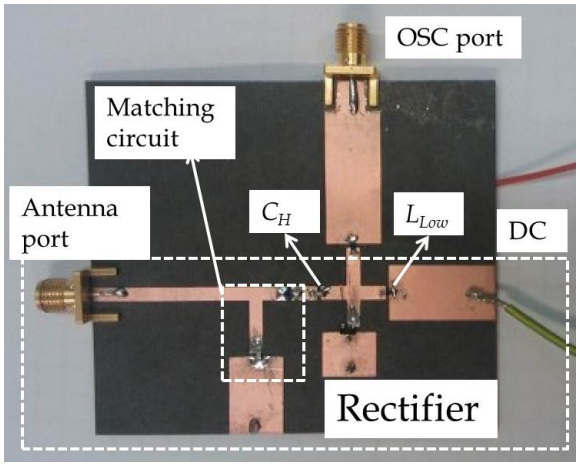

Fig. 5.2: Manufactured rectifier prototype.

5.1.2 Measurement setup

The schematic layout of the measurement setup is shown in Fig. 5.3 (a). A continuous wave (CW) is generated by a network analyzer (Agilent 8753ES) and it is fed to the antenna port of the sensor. The rectified DC voltage is measured with a multimeter. A photograph of the measurement setup is shown in Fig. 5.3 (b).

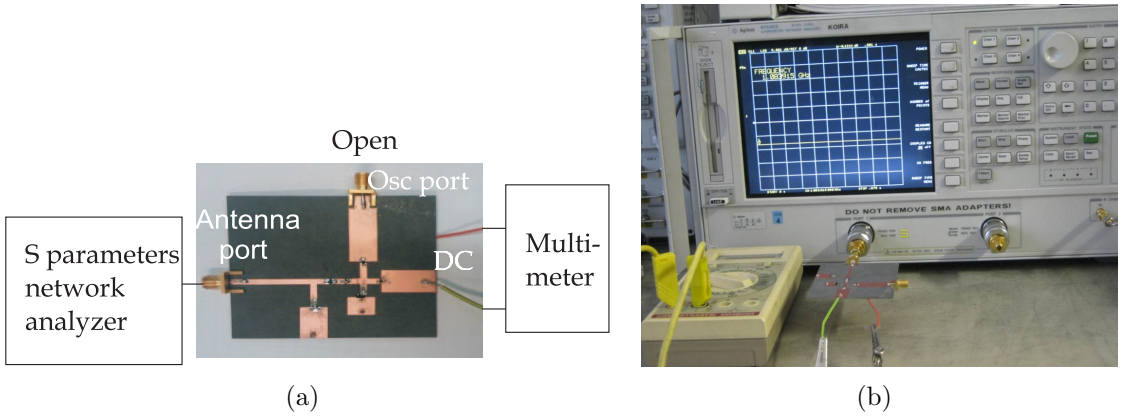

Fig. 5.3: (a) A schematic layout of the measurement setup for measuring the rectified DC voltage; (b) Measurement setup for characterizing the rectifier.

5.1.3 Measured and simulated results

Fig. 5.4 shows the measured and simulated reflection coefficient of the rectifier prototype. The reflection coefficient is measured at low power level (−15 dBm) to ensure the operation in the small signal region. The best matching is obtained at 1.085 GHz in measurement. The shift of the matching frequency as compared to the design frequency (1 GHz) is mainly due to the grounding vias in transmission lines TL_3 and TL_8 that were found to have a significant effect in the simulation (see Fig. 5.4). In the following analysis, 1.085 GHz excitation signal is used because the circuit operates best at that frequency.

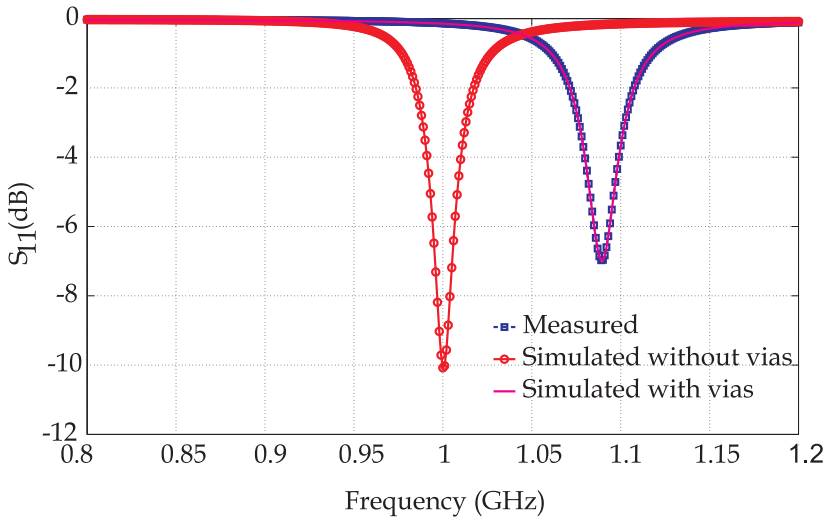

Fig. 5.4: Measured and simulated reflection coefficient of the rectifier.

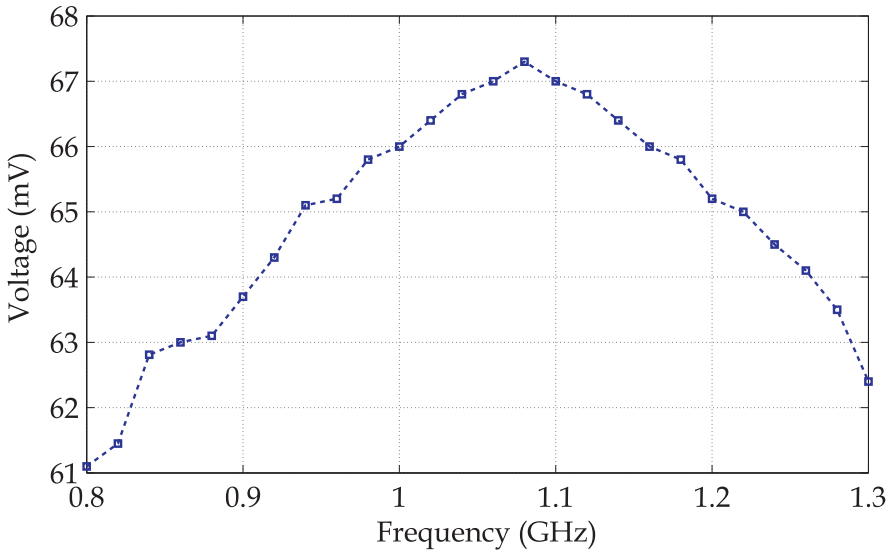

Fig. 5.5: Measured DC voltage generated by the rectifier as a function of input frequency. The input power is –10 dBm.

Fig. 5.5 shows the DC voltage generated by the rectifier as a function of the input frequency, when input power is –10 dBm. The rectifier generates the maximum voltage at the frequency where it is matched well. The simulated and measured rectification responses as a function of input power are shown in Fig. 5.6.

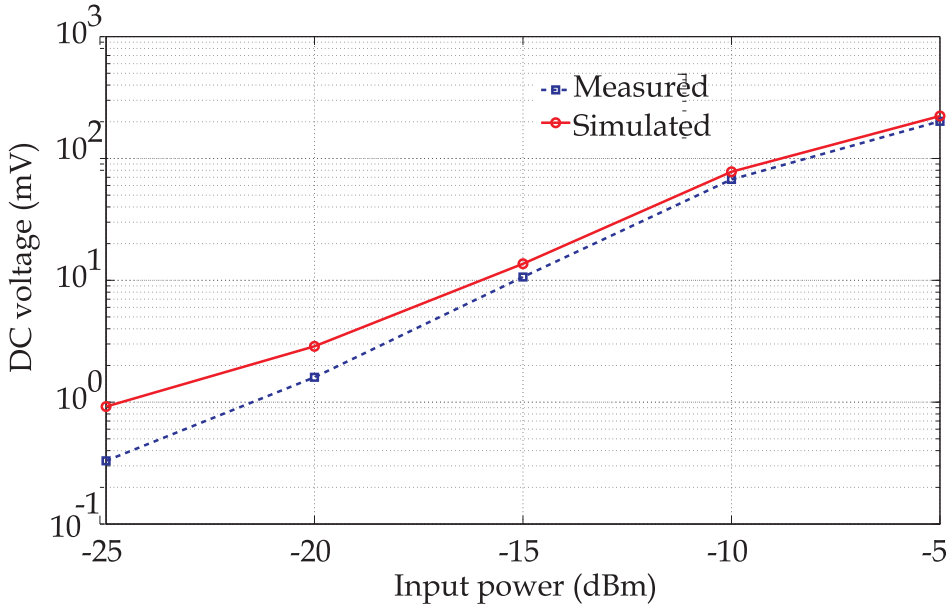

Fig. 5.6: Simulated and measured rectified voltage as a function of the input voltage at 1.085 GHz.

The simulated results align almost perfectly with the measured one at 1.085 GHz above −15 dBm. Below −15 dBm, simulated DC voltage is a little bit higher than the measured. During the design of the diode matching circuit, an input power of −15 dBm was considered , which might not satisfy the small signal condition for the diode. Therefore, in lower power level simulation results varies from the measured one. For designing a matching circuit, input power of −15 dBm is chosen randomly.

5.2 Oscillator

5.2.1 Oscillator prototype

A simple Colpitts oscillator was implemented in practice in order to verify the analytical and simulation models. The oscillator output voltage as a function of input voltage was first simulated with the ADS software using the harmonic balance simulation. A SPICE (LEVEL 2) model is used for the MOSFET in the simulation. Inductors are simulated using InDQ2 (inductor with Q) model, which is available in ADS. The schematic circuit of the simulated oscillator is shown in Fig 5.7 (a). The component values used in the simulation and measurement are listed in Table 5.3.

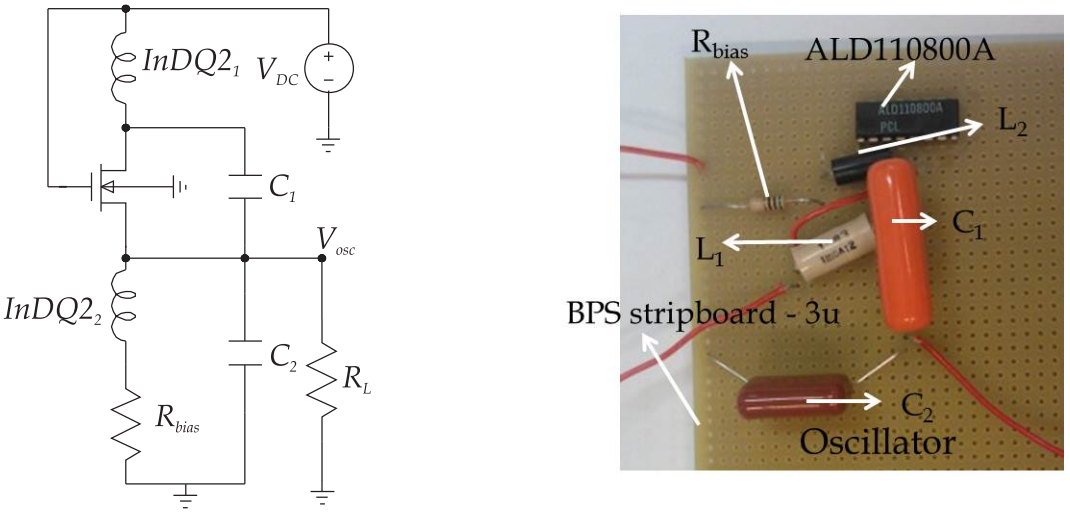

(a) (b)

Fig. 5.7: (a) Oscillator simulation model (including losses); (b) Measured Oscillator prototype.

Next, the oscillator circuit was implemented by using the BPS stripboard-3u. An ALD110800A matched pair MOSFET was used for designed oscillator. The oscillator prototype is shown in Fig. 5.7 (b). With the aim of generating a signal at 100 kHz, feedback inductor $InDQ2_1 = 1$ mH, inductor connected at the transistor source $InDQ2_2 = 10$ mH, as well as capacitors $C_1 = 3.3$ nF and $C_2 = 16$ nF are used. The series resistance and quality factor of the inductors are given in Table 5.3.

Table 5.3: Parameters used in the oscillator simulation and measurement

Inductor of $InDQ2_1$	$InDQ2_1(L) = 1$ mH
Series resistance of $InDQ2_1$	$InDQ2_1(R) = 12\ \Omega$
Quality factor of $InDQ2_1$ at 100 kHz	$InDQ2_1(Q) = 55$
Inductor of $InDQ2_2$	$InDQ2_2(L) = 10$ mH
Series resistance of $InDQ2_2$	$InDQ2_2(R) = 51\ \Omega$
Quality factor of $InDQ2_2$ at 100 kHz	$InDQ2_2(Q) = 48$
Capacitor	$C_1 = 3.3$ nF
Capacitor	$C_2 = 16$ nF
Load resistance	$R_L = 0.5\ \mathrm{M}\Omega$
Resistance (bias)	$R_{bias} = 50\ \Omega$

5.2.2 Measurement setup

The oscillator is tested by measuring its output AC voltage as a function of input DC voltage. Fig. 5.8 shows a schematic layout of the measurement setup. DC voltage is supplied by a DC voltage supply, and the waveform is captured with an oscilloscope.

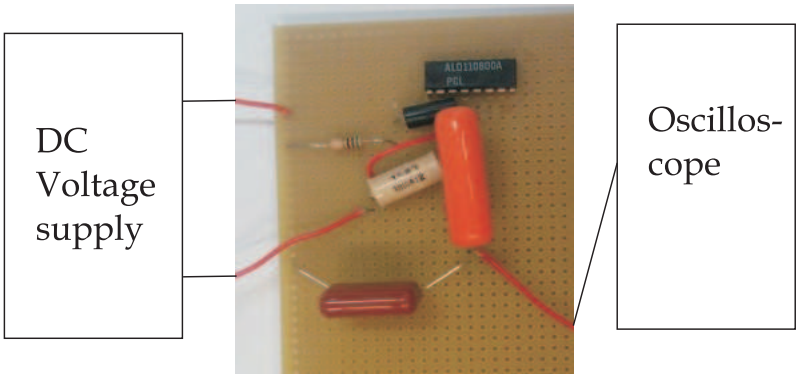

Fig. 5.8: A schematic layout of the measurement setup for measuring the oscillator output.

5.2.3 Measured and simulated results

Fig 5.9 shows the simulated and measured output voltage of the oscillator as a function of the input voltage. According to the simulation, oscillation is sustained when the input DC voltage is above 1.07 V, whereas the turn on voltage is 1.15 V in the measurement. The difference between simulated and measured result is 0.08 V. Fig. 5.9 shows that the simulated output voltage of the oscillator aligns well with the measured one at voltages below 2 V. Above 2 V, the simulated voltage is a little bit higher than the measured voltage. This discrepancy likely occurs due to the transistor SPICE (LEVEL 2) simulation model. According to the manufacturer, the MOSFET model ALD110800 is used in the simulation generally reflects the typical baseline specification of the real device but certain aspects of performance are not modeled fully [63].

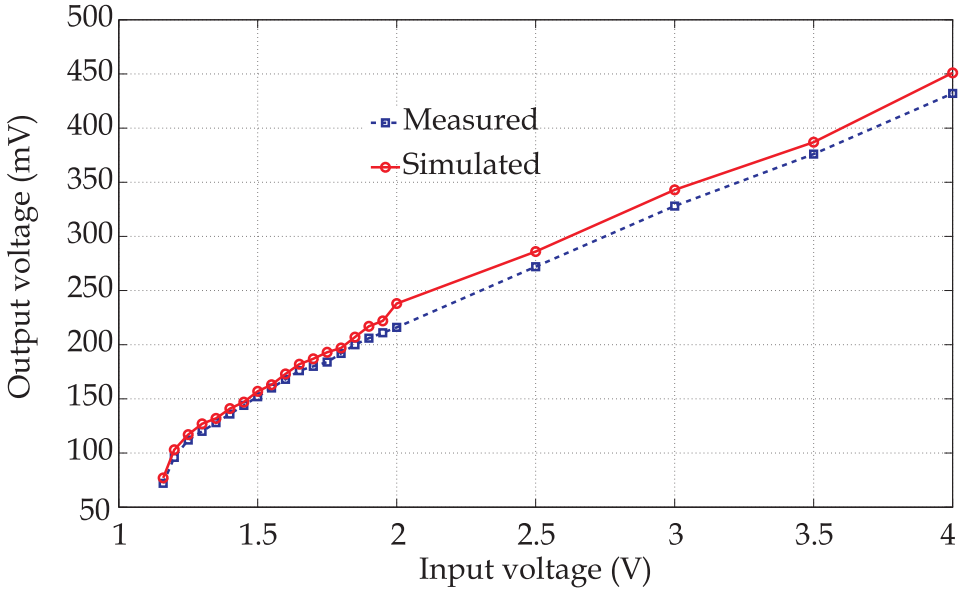

Fig. 5.9: Comparison between the simulated and measured output voltage of the oscillator as a function of input voltage predicted by harmonic balance simulation.

The measured waveform captured with an oscilloscope is shown in Fig. 5.10. Fig. 5.10 shows a 656 mV peak-to-peak signal at around 100.874 kHz when the input voltage is 3 V. The measured oscillation frequency (100.874 kHZ) matched well with the simulated oscillation frequency (100 kHz).

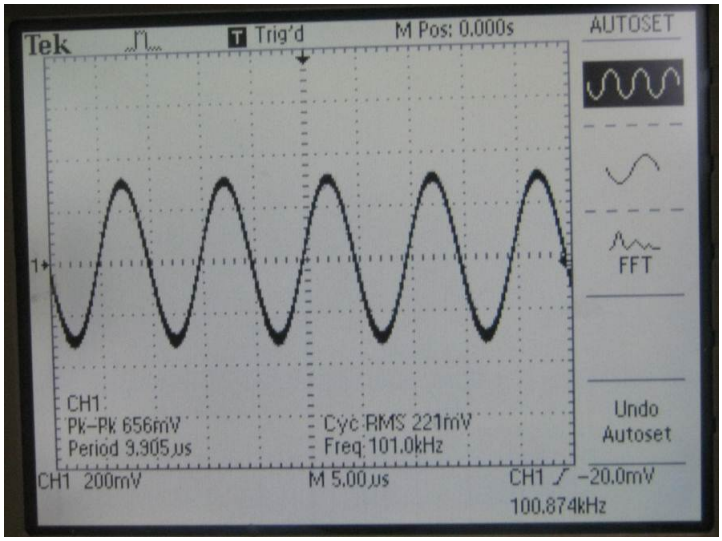

Fig. 5.10: Measured waveform of the signal when input voltage is 3 V.

5.3 Modulator

In order to realize a sensor utilizing the backscattering principle, a modulator is needed. A simple modulator circuit is simulated and measured, and the results are discussed in this Section. A rectifier circuit is also used as a part of the modulator circuit. An RF choke is used as a band-pass filter. It allows the oscillator frequency to pass through and stop other frequencies. The signals from both sources are mixed in the diode which generates current at the difference frequency. The current at the difference frequency then generates a voltage that depends on the circuit impedance as shown in Section 4.3.

5.3.1 Modulator Prototype

The purpose of the simulation is to ensure that analytical model is relevant and accurate. The schematic circuit of the simulated model is shown in Fig. 5.11, in which simulation model of the modulator consist of a rectifier circuit with two transmission lines TLM_1 ($L = 7.2$ mm and $W = 2.3$ mm) and TLM_2 ($L = 30$ mm and $W = 10$ mm), an inductor ($L_{mlow} = 43$ nH) as a band-pass filter and a voltage source which represents the oscillator. A zero bias Schottky diode is used as the mixer. The component values used in the simulation and measurement are listed in Table 5.1. The modulated power reflected by the sensor is simulated with the ADS software using harmonic balance simulation.

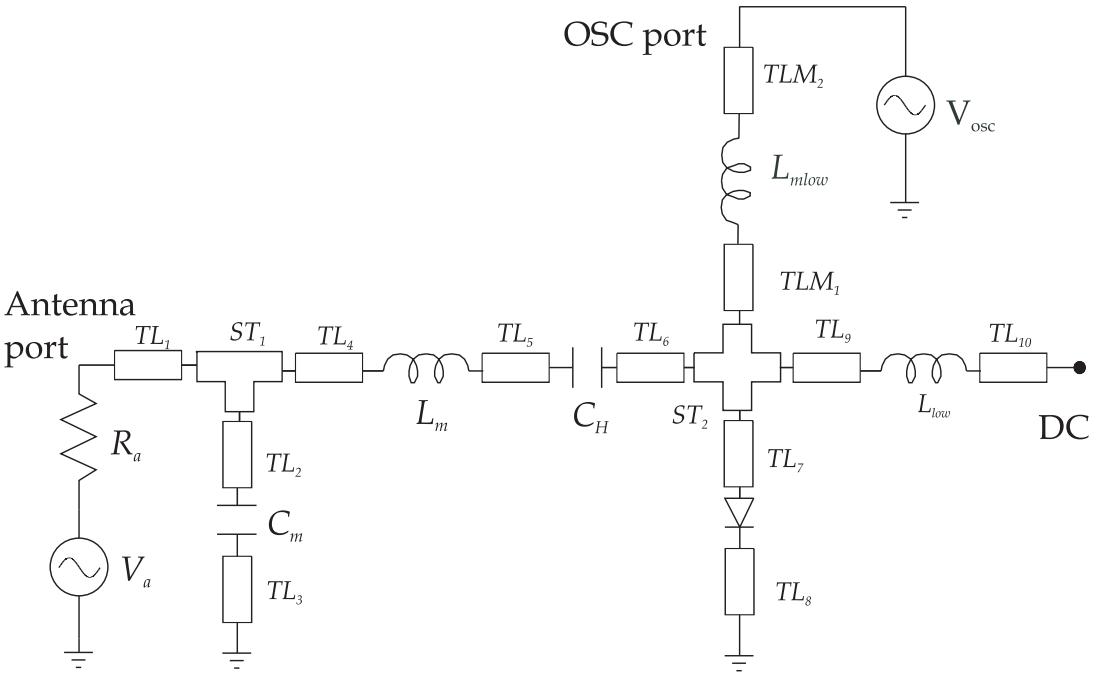

Fig. 5.11: Schematic circuit of the modulator simulation model.

The modulator circuit is implemented in practice to ensure that the analytical and simulation models are relevant and accurate. The modulator circuit utilizes the rectifier circuit to reflect power back to the reader. For this reason, the modulator circuit layout has been generated and fabricated with the rectifier circuit. A 50 Ω SMA connector was soldered in the OSC port to supply the oscillation voltage. A photograph of the modulator prototype is shown in Fig. 5.12.

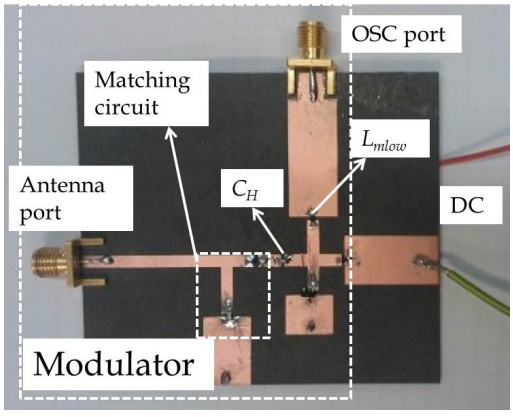

Fig. 5.12: Modulator prototype, where the rectifier circuit is also used as a part of the modulator

5.3.2 Measurement setup

The modulator is tested by measuring the modulated reflected power by the sensor as a function of oscillator output voltage, while the input power of the sensor is kept constant. A schematic layout of the measurement setup is shown in Fig. 5.13 (a). The oscillator output voltage is generated with a signal generator (Wavetek 395) at 10 kHz and fed to the OSC port. The reflected power of the sensor is measured with a network analyzer (Agilent E8363A). A photograph of the measurement setup is shown in Fig. 5.13 (b).

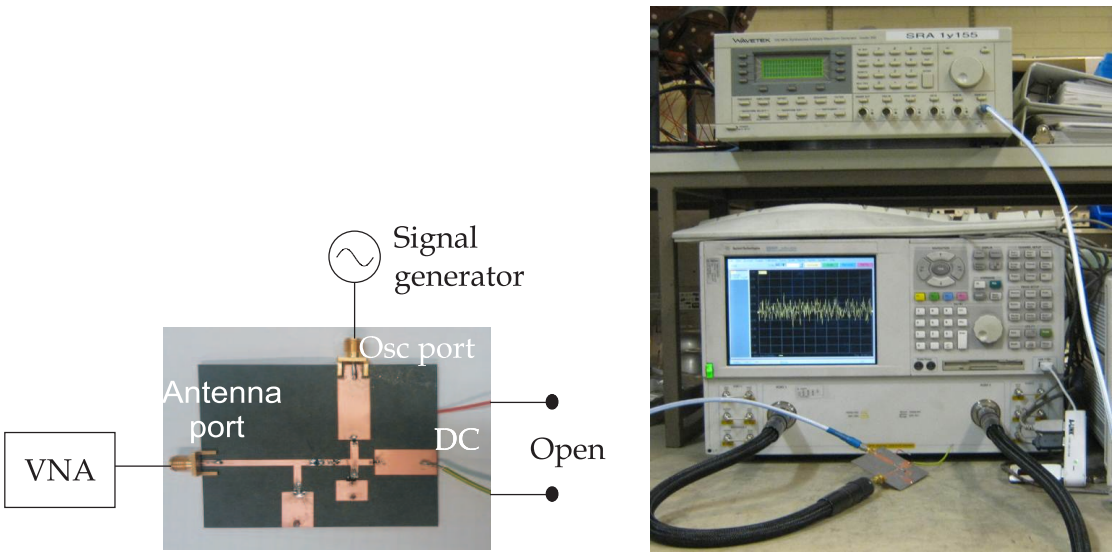

Fig. 5.13: (a) A schematic layout of the measurement setup for measuring the backscattering response of the sensor; (b) Measurement setup for measuring the backscattering response of the sensor.

5.3.3 Measured and simulated results

The reflected power of the sensor was studied by sweeping the oscillation output voltage, keeping the oscillation frequency and input power constant. Fig. 5.14 shows the simulated and measured reflected power of the sensor as a function of output voltage of the oscillator. The input power of the sensor is -10 dBm and an oscillation frequency of 10 kHz is used in the measurement. There is an offset between the measured and simulated curves, but they exhibit similar shape.

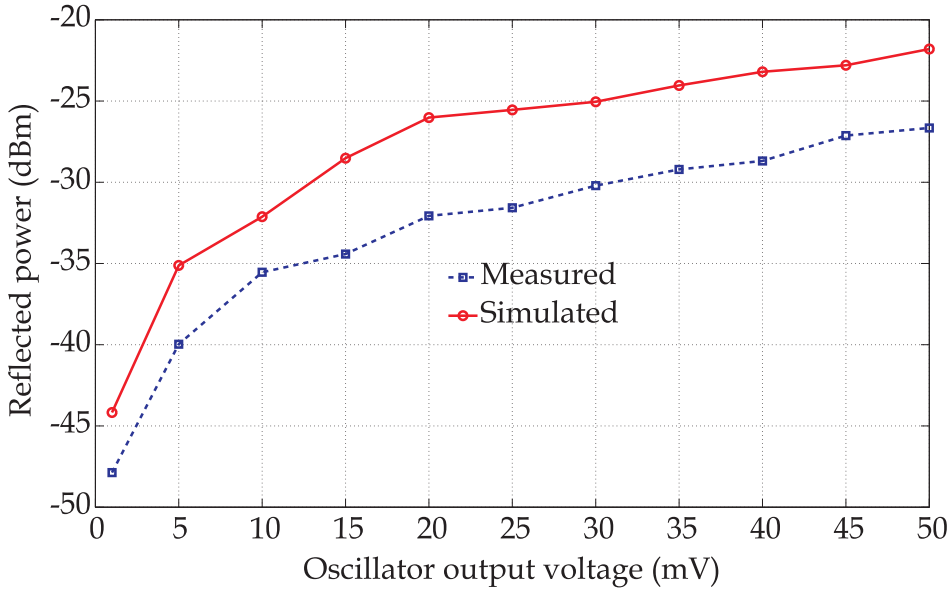

Fig. 5.14: Simulated and measured backscattering response of the sensor as a function of output oscillator voltage. The input power is –10 dBm and the oscillation frequency 10 kHz.

The deviation between the measured and simulated curves is likely due to the cable loss and the impedance mismatch between the OSC port and the diode. In the measurement, the oscillator output voltage has been generated with the signal generator and fed through the OSC port. The signal generator might introduce resistance in the OSC port, which is responsible for creating the impedance mismatch between the diode and OSC port. Therefore, the measured results varied from the simulated one.

5.4 Observation on the experiments

In the above discussion, discrete parts of the sensor were simulated and experimentally characterized to predict the performance of the sensor. Simulated and measured results show good agreement, which ensures that the analytical and simulation models are relevant and accurate. The rectifier result shows a relation between the sensor input power and generated DC voltage. Using this relation, it is possible to find out the required input power of the sensor. An oscillator is designed and measured to characterize the oscillator performance parameters. The designed oscillator required a minimum supply voltage of 1.15 V to start the oscillation which

makes it infeasible for use in a passive wireless sensor. During the design of the oscillator, some key features are realized which should be considered when designing an oscillator. The power consumption of an oscillator can be made arbitrarily low by decreasing the capacitive divider ratio and increasing the quality factor (Q) of the feedback inductor. In this thesis, a new oscillator considering these things was not designed but it is possible to design an oscillator which can operate with a minimum supply voltage of below 20 mV. In the modulator section, the modulated reflected power of the sensor is predicted as a function of oscillator output voltage, which is useful for predicting the read-out distance of the sensor. The read-out distance was not calculated and measured in this thesis, but the sensor could potentially be read-out across much larger distance compare to the existing passive wireless sensors. Combining all these relations, the modulated reflected power of the sensor as a function of input power can be predicted.

6 Conclusion

Current passive wireless sensors cannot simultaneously provide sensing and the sophisticated features of RFID. This thesis studied the possibility to equip an RFID tag with an LC-oscillator and sensor element in order to enable the sophisticated features of RFID and the possibility to measure external quantities without reducing the read-out distance. The concept of the sensor, which consists of three main parts: a rectifier, an oscillator and a modulator, is analyzed and demonstrated experimentally. When the sensor is illuminated with one frequency, it emits the sensor data to the reader at one of the side band frequencies.

When the sensor is interrogated with a continuous wave (CW), the rectifier generates the DC supply for the oscillator. Utilizing the rectified DC voltage, the oscillator produces a low frequency sinusoid which drives the modulator. In this thesis, theoretical equations for various properties of the different sensor parts were derived. Rectified DC voltage as a function of input power is derived to describe the input DC voltage of the oscillator. For the oscillator, an analytical equation for the output voltage is reviewed to predict the oscillator output voltage as a function of input DC voltage. In addition, a theory to predict the oscillator power consumption is established, and other oscillation parameters such as oscillation condition and frequency stability are reviewed. Furthermore, an analytical equation is derived for the modulator to describe the reflected power of the sensor, which can be used to predict the achievable detection distance.

The derived analytical equations are verified by simulation using ADS software with harmonic balance simulation. Finally, each part of the sensor is implemented in practice to ensure the relevance and accuracy of the analytical and simulation models, and to make sure that these models have sufficient parameters for predicting the performance of the sensor. The rectifier and modulator circuit layout has been generated with ADS software. The prototype with the simulated circuit elements is fabricated in RAD laboratory. The oscillator prototype is made by soldering the components on a stripboard. Prototypes are measured and compared with the simulation results. The comparison shows that the measured responses match well with the simulation results.

In summary, rectifier, oscillator and modulator for the transponder are analytically derived to predict the performance of the sensor. The concept is experimentally demonstrated by designing and implementing each part of the sensor. The results of this thesis show that this concept is feasible but further development is needed to obtain a passive sensor with larger read-out distance and smaller power consumption.

In the near future, the sensor performance will be measured integrating all three parts together. The power consumption of the sensor can be reduced by designing an oscillator which can operate at ultra low voltage. Furthermore, for oscillation, most of the power consumption takes place at the feedback inductor and the capacitive divider. So, a mathematical equation could be developed in future to find out the optimal inductor value and capacitive divider ratio for the oscillation. The oscillator circuit inductor will be replaced with a crystal to achieve higher frequency stability. In addition, a sensor element will be attached to the oscillator circuit for measuring external quantity. In the final stage, the sensor will be integrated into an existing RFID tag so that this could enable the features of identification and the possibility to measure an external quantity with larger read-out distance and reduced power consumption.

References

[1] V. Viikari and H. Seppä, "RFID MEMS sensor concept based on intermodulation distortion," *IEEE Sensor Journal*, vol. 9, no 12, pp. 1918–1923, Dec. 2009.

[2] H. Stockman, "Communication by means of reflected power," *Proceedings of the Institute of Radio Engineering*, vol. 36, no 10, pp. 1196–1204, Oct. 1948.

[3] K. Finkenzeller, *RFID Handbook*, Munich, John Wiley & Sons Inc., 2003.

[4] S. Zhan, *Analysis and Design of Metal-Surface Mounted Radio Frequency Identification (RFID) Transponder*, Graduate Thesis and Dissertations, Iowa State University, Ames, lowa, USA, 2008.

[5] R. F. Harrington, "Theory of loaded scatterers," *Proceedings of the IEEE*, vol. 111, no. 4, pp. 617–623, Apr. 1964.

[6] J. H. Vogelman, "Passive data transmission techniques utilizing radar echoes," US Patent 33914041968, Jul. 2, 1964.

[7] J. Landt, "The history of RFID," *IEEE Potentials*, vol. 24, no. 4, pp. 8–11, Oct.–Nov. 2005.

[8] http://www.ams.com/eng/Press/Press-Released/RFID-Sensor-Tags (Cited Oct. 20, 2013).

[9] R. Steindl, A. Pohl, and F. Seifert, "Impedance loaded SAW sensors offer a wide range of measurement opportunities," *IEEE Transactions on Microwave Theory and Techniques*, vol. 47, no 12, pp. 2625–2629, Dec. 1999.

[10] S. Saati, R. Varma, M. S. Humayun, and T. Yu-Chong, "Wireless intraocular pressure sensing using microfabricated minimally invasive flexible-coiled LC sensor implant," *IEEE Journal of Microelectromechanical System*, vol. 19, no 4, pp. 721–734, Aug. 2010.

[11] J. Song, V. Viikari, N. Pesonen, I. Marttila, and H. Seppä, "Optimization of wireless sensors based on intermodulation communication," *IEEE Transactions on Microwave Theory and Techniques*, vol. 61, no 9, pp. 3446–3452, Sep. 2013.

[12] R. M. White, "A sensor classification scheme," *IEEE Transactions on Ultrasonics, Ferroelectrics and Frequency Control*, vol. 34, no 2, pp. 124–126, Mar. 1987.

[13] OMEGA Engineering Technical Reference, [Online]. Available : http://www.omega.com/prodinfo/wirelesssensors.html (Cited Oct. 20, 2013).

[14] M. P. da Cunha, R. J. Lad, P. Davulis, A. Canabal, T. Moonlight, S. Moulzolf, D. J. Frankel, T. Pollard, D. Mccann, E. Dudzik, A. Abedi, D. Hummels, and G. Bernhardt, "Wireless acoustic wave sensors and systems for harsh environment application," *Proceedings of the IEEE Topical Conference on Wireless Sensors and Sensors Networks (WiSNet)*, Phoenix, AZ, 14–16 Jan. 2011, pp. 41–44.

[15] J. English and M. Allen, "Wireless micromachined ceramic pressure sensors," *Proceedings of the 12th IEEE International Conference on Micro Electro Mechanical System. Microelectromech*, Orlando, FL, 1999, pp. 511–516.

[16] B. Dixon, V. Kalinin, J. Beckley, and R. Lohr, "A second generation in-car tire pressure monitoring system based on wireless passive SAW sensors," *Proceedings of 2006 IEEE Frequency Control Symposium and Exposition*, Miami, FL, Jun. 2006, pp. 374–380.

[17] J. Song, *On Optimazation and Read−out Resolution of the Zero Power Sensor*, Master's Thesis, Aalto University School of Electrical Engineering, Finland, 2012.

[18] N. Björn, *Energy Efficient Protocols For Active RFID*, Doctoral Thesis, Department of Computer Science and Engineering, Chalmers University of Technology, Sweden, 2010.

[19] A. P. Sample, D. J. Yeager, P. S. Powledge, A. V. Mamishev, and J. R. Smith, "Design of an RFID-based battery-free programmable sensing platform," *IEEE Transactions on Instrumentation and Measurement*, vol. 57, no. 11, 2008, pp. 2608–2615.

[20] R. Angles,"RFID technologies: Supply-chain application and implementation issues," *Information System Management*, vol. 22, no. 1, pp. 51–65, Dec. 2006.

[21] D. Musiani, K. Lin, and, T. S. Rosing, "Active sensing platform for wireless structural health monitoring," *6th International Symposium on Information Processing in Sensor Network (IPSN 2007)*, Cambridge, MA, 25–27 Apr. 2007, pp. 390–399.

[22] G. Werner-Allen, K. Lorincz, M. Welsh, O. Marcillo, J. Johnson, M. Ruiz, and J. lees, "Deploying a wireless sensor network on an active volcano," *IEEE Internet Computing*, vol. 10, no. 2, pp. 18–25, Mar./Apr. 2006.

[23] TagSense, [online]. Available : http://www.tagsense.com (Cited Oct. 20, 2013).

[24] R. Jedermann and W. Lang, "Semi-passive RFID and beyond: steps towards automated quality in the food chain," *International Journal of Radio Frequency Identification Technology and Application*, vol. 1, no. 3, pp. 247–259, 2007.

[25] R. Jedermann, L. Ruiz-Garcia, and W. Lang, "Spatial temperature profiling by semi-passive RFID loggers for perishable food transportation," *Computers and electronics in Agriculture.*, Vol. 65, no. 2 pp. 145–154, Mar. 2009.

[26] V. Viikari, H. Seppä, and D. W. Kim, "Intermodulation read-out principle for passive wireless sensors," *IEEE Transactions on Microwave Theory and Techniques*, vol. 59, no 4, pp. 1025–1031, Apr. 2011.

[27] R. Weinstein, "RFID: A technical overview and its application to the enterprise," *IT Professional*, vol. 7, no. 3, pp. 27–33, May-Jun. 2005.

[28] R. Want, "Enabling ubiquitous sensing with RFID," *Computer*, vol. 37, no. 4, pp. 84–86, Apr. 2004.

[29] Y. Anjie and Y. Jianwei, "Research on application of RFID technology in the automobile parts logistics," *2011 International Conference on Consumer Electronics, Communications and Networks (CECNet)*, XianNing, 16–18 Apr. 2011, pp. 602–605.

[30] Y. J. Jing, and Z. Y. Chuan, "Research on automobile supply chain model based on RFID," *Logistics Technology*, 2007, vol. 26, no. 9, pp. 93–95.

[31] S. S. Ahmet, *Passive Wireless Sensing Strategies or High Frequency Biomedical Sensing Application,* Doctoral Thesis, University Of Minnesota, U.S, Dec. 2006.

[32] V. Viikari, J. Song, and H. Seppä, "Passive wireless sensor platform utilizing a mechanical resonator," *IEEE Sensors Journal*, vol. 13, no. 4, pp. 1180–1186, Apr. 2013.

[33] J.C. Butler, A.J. Vigliotti, F.W. Verdi and S. M. walsh, "Wireless passive, resonant-circuit, inductively coupled, inductive strain sensor," *Sensors and Actuators A: Physical*, vol. 102, no. 1–2, pp. 61–66, Dec. 2002.

[34] J. Voutilainen, *Methods and Instrumentation for Measuring Moisture in Building Structure,* Doctoral Thesis, Helsinki University and Technology, Espoo, finland, 2005.

[35] K. Takahata, A. DeHennis, K.D. Wise, and Y.B. Gianchandani, "A wireless microsensor for monitoring flow and pressure in a blood vessel utilizing a dual-inductor antenna stent and two pressure sensors," *17th IEEE International Conference on Micro Electro Mechanical Systems(MEMS)*, pp. 216–219, Sep. 2004.

[36] A. Phol, "A review of wireless SAW sensors, " *IEEE Transactions on Ultrasonics, Ferroelectrics, and Frequency Control*, vol. 47, no. 2, Mar. 2000, pp. 317–332.

[37] G.C. Frye, R.J. Kottenstette, E.J. Heller, C.J. Brinker, S.A. Casalnuovo, Alan Sellinger, N.K. Raman, and, Lu Yunfeng, "Optimizing surface acoustic wave sensors for trace chemical detection, "*1997 International Conference on Solid State Sensors and Actuators (TRANSDUCERS '97)*, Chicago, 16–19 Jun. 1997, vol. 2, pp. 1323–1326.

[38] RFID and temperature sensing utilizing SAW technology, [online]. Available : http://www.rfsaw/Pages/default.aspx (Cited Oct. 20, 2013).

[39] V. Viikari, J. Chisum and H. Seppa, "Wireless passive photo detector for insect tracking," *Microwave and Optical Technology Letters*, vol. 52, no. 10, pp. 2312–2315, Oct. 2010.

[40] E. A. Capaldi, A.D. Smith, J. L. Osvorne, S. E. Fahrbach, S. M. Farris, D. R. Reynolds, A. S. Edwards, A. Martin, G. E. Robinson, G. M. Poppy, and J. R. Riley, "Ontogeny of orientation flight in the honeybee revealed by harmonic radar," *Nature*, vol. 403, pp. 537–540, 2000.

[41] G. Boiteau and B. Colpitts, "Electronic tags for the tracking of insects in flight: Effect of weight on flight performance of adult Colorado potato beetles," *Entomologia Experimentalis et Applicata*, vol. 100, pp. 187–193, 2001.

[42] J. L. Osvorne, S. J. Clark, R. J. Morris, I. H. Williams, J. R. Riley, A.D. Smith, D. R. Reynolds, and A. S. Edwards, "A landscape-scale study of bumblebee foraging range and constancy, using harmonic radar," *Journal of applied Ecology*, vol. 36, pp. 519–533, 1999.

[43] G. P. Svensson, P. G. Valeur, D. R. Reynolds, A. D. Smith, J. R. Riley, T. C. Baker, G. M. Poppy, and C. Löfstedt, "Mating disruption in Agrotis segetum monitored by harmonic radar," *Entomologia Experimentalis et Applicata*, vol. 101, pp. 111–121, 2001.

[44] B. G. Colpitts, and G. Boiteau, "Harmonic radar transceiver design: miniature tags for insect tracking," *IEEE Transactions on Antennas Propagation*, vol. 52, pp. 2825–2832, 2004.

[45] E.T. Cant, A.D. Smith, D.R. Reynold and J.L. Osborne, "Tracing butterfly paths across the landscape with harmonic rader," *Proceedings of the Royal Society Biological Science*, vol. 272, no. 1565, pp. 785–790, Apr. 2005.

[46] J.R. Riley and A.D. Smith,"Design consideration for an harmonic radar to investigate the flight of insects at low altitude," *Computers and Electronics in Agriculture.* Amsterdam, The Netherlands: Elsevier, 2002 vol. 35, pp. 151–169.

[47] H. Staras and J. Shefer, "Harmonic radar detecting and ranging system for automotive vehicles," US patent 3,781,879 (1972).

[48] J. Saebboe, V. Viikari, T. Varpula, H. Seppä, Cheng Shi, M. Al-Nuaimi, P. Hallbjorner, A. Rydberg, "Harmonic automotive radar for VRU classification," *International Radar Conference - Surveillance for a Safer World,*, Bordeaux, 12–15 Oct. 2009, pp. 1–5.

[49] Tracking avalanche victims [Online]. Available : http://www.recco.com (Cited Oct. 20, 2013).

[50] V. Viikari and H. Seppä, "RFID MEMS sensor concept based on intermodulation distortion," *IEEE Sensors Journal*, vol. 9, no. 12, pp. 1918–1923, Dec. 2009.

[51] D.E.N. Davies, and H. Makridis, "Two-frequency secondary radar incorporating passive transponders," *Electronics Letters*, vol. 9, no. 25, pp.592–593, Dec. 1973.

[52] V. Viikari, H. Seppä, T. Mattila, and A. Alastalo,"Wireless ferroelectric resonating sensor," *IEEE Transactions on Ultrasonics, Ferroelectrics and Frequency Control*, vol. 57, no. 4, pp. 785–791, Apr. 2010.

[53] S. R. Ardali, S. G. Samani, and B. Arzanifar, "Oscillation amplitude analysis of MOS Hartley oscillator using a general model," *Journal Integrated Circuit and System*, vol. 6, no. 1, pp. 60–67, 2011.

[54] D. M. Pozar, *Microwave Engineering*, John Wiley & Sons, 4^{th} edition, 2012.

[55] R. Vaughan and J. B. Anderson, *Channels, Propagation and Antennas for Mobile Communication*, The IEEE Electromagnetic Wave Series 50, 2003.

[56] K. Stadius, *Integrated RF oscillator and LO signal generation circuits,* Doctoral Thesis, Department of Micro and Nanosciences, Aalto University, Finland, 2010.

[57] G. Gonzalez, *Foundation of oscillator circuit design*, Artech House, INC. Boston, London 2007.

[58] A. S. Sedra, and K. C. Smith, *Microelectronic Circuits*, Oxford University Press, 5^{th} edition, New York, 2004.

[59] D. O. Pederson and K. Mayaram, *Analog Integrated Circuits for Communication: Principles, Simulation and Design.*, Springer, London, 2007.

[60] K. Mayaram and D. O. Pederson, "Analysis of MOS transformer-coupled oscillator," *IEEE Journal of Solid-State Circuits*, vol. 22, no. 6, pp. 1155–1162, Dec. 1987.

[61] T. H. Lee, *The Design of CMOS Radio-Frequency Integrated Circuits*, Cambridge University Press, 2004.

[62] Avago Technologies, "HSMS-286x series Datasheet," [Online]. Available : http://www.avagotech.com/ (Cited Oct. 20, 2013).

[63] Advanced Linear Devices, INC., "ALD110800 Datasheet," [Online]. Available : http://www.aldinc.com/ (Cited Oct. 20, 2013).